Supplementary information

I. Shortened Method Section

Data Mining and statistical analysis - Petrological and geochemical databases provide access to several tens of thousands rocks and minerals analyses covering most of the Earth's history. Data mining techniques allow the exploration of these datasets to uncover hidden patterns and trends over time periods several tens of millions to hundreds of million years (Keller & Schoene, 2012; Tang et al., 2016). These global trends are commonly tainted by statistical uncertainties and their interpretation is non-unique, which renders these studies unpopular in the community of petrologists. The most skeptical believe that by using lots of data, we either ignore the complexities in magmatic systems or that the "mean" in petrology has no meaning because it would mask the natural variability in T (or depth) of partial melting and crystallization in igneous rocks from widely different geological environments. The key then is to ensure that we can capture relevant insight into secular change while taking advantage of more detailed studies concerning the processes that lead to a heterogeneous rock record (see **Extended Method - section 3** below). The other valid criticisms people make are that we need to be really careful to address sampling bias and to address the effect of mixing rocks from different tectonic settings.

In order to derive magmatic temperature estimates and map its trend over the past 600 Myr, we compiled data from GEOROC [at https//www.georoc.mpch-mainz.gwdg.de/georoc/], a database including over 16 million data points derived from geo-referenced bulk-rock composition and associated mineral analysis. More than 92 % of the samples correspond to volcanic rocks and >98% of the minerals present in our database have been sampled in volcanic rocks. Results for global mean intensive (geochemical) and extensive (T, Tp) values with time are reported with associated 1-standard-error of the sample mean at 50 Myr intervals. The standard error of the sample mean, which is the standard deviation divided by the square root of the sample size, gives us an estimate of how far away our sample error might be form the true population mean. Accordingly, the population mean is within 2 times the standard error from the sample mean about 95% of the time. These means were generated by Monte Carlo analysis with bootstrap resampling techniques to mitigate sampling bias (see **Extended Method - section 1** below). A polynomial curve (N, R^2) fitting the bootstrapped values was reported on the graphs.

Magma temperature - Following the methods of Putirka (2008), built on a comprehensive review of thermo-barometers for magmatic rocks, we compared different magmatic mineral compositions with bulk rock compositions using experimentally derived thermometers to obtain temperatures of crystallization. To unravel the thermal evolution of magmas we have used only the most robust thermometers as proposed in Putirka (2008) and Ridolfi and Renzulli (2012). While magmatic temperatures can be confidently calculated from any silicate mineral in equilibrium with its hosting magma (Putirka, 2008), the calculation of pressure suffers larger uncertainties and was not considered here (see **Extended Method - section 2** below).

Primary magma (lava) compositions and mantle Tp values were obtained for our database using the PRIMELT3 MEGA software (Herzberg & Asimow, 2015). The software is calibrated by anhydrous melting experiments on fertile peridotite, and its application to lavas assumes a similar fertile and dry peridotite source. Uncertainties in fertile peridotite composition do not propagate to significant errors in mantle Tp (Herzberg & Asimow, 2008). Conversely, melting of wet peridotite is likely to propagate to excessively elevated MgO and mantle Tp. We discuss this point in the **Extended Method - section 3**. PRIMELT automatically filters and excludes all samples that have undergone clinopyroxene and or plagioclase fractionation as indicated by depletion of CaO and Al_2O_3. Finally, our solutions of calculation have been filtered according to a graphic procedure (Herzberg & Asimow, 2008), leading to reduced uncertainties that arise from pyroxenite source lithology, source volatile content from metasomatized peridotite, and clinopyroxene fractionation. The remaining samples (271) were assumed to have been affected only by variable amounts of olivine addition and subtraction (Figure 16 SI).

As a complementary approach, magmatic rocks have been analyzed with the olivine- and glass-based thermometers of Putirka (2008) to obtain information on mantle-derived primary magma compositions from a largest range of mantle rocks composition. More than 5,600 successful Tp solutions have been obtained for a total of > 14,300 olivine-bearing samples (Figure 17 SI).

Chemistry of magmatic systems - In tholeiitic magmatic systems evolving at shallow level in the crust, the sequence of crystallization for magmatic minerals (i.e. the Bowen's Reaction Series) and their compositions depend mainly on the composition of the parental magma and its temperature (Putirka, 2008). Feldspars form a continuous series, evolving from calcium to sodium-rich term as the *P* and *T* decrease. Conversely, Fe-Mg magmatic minerals form a discontinuous series in which olivine stabilizes early, followed by the growth of pyroxene then amphibole and biotite if water is available in the magma. The Mg-Fe substitutions in olivine and pyroxene are *T*-sensitive, with Mg-rich endmembers stabilizing at higher temperature in more Mg-rich magmas (Figure 9 and 14 SI**)**. It is noteworthy that basaltic melts evolving in deeper magmatic sources, often in the presence of fluids (e.g. calc-alkaline magmatic systems), are characterized by a different sequence of crystallization, with the plagioclase, clinopyroxene (*cpx*) and olivine crystallizing simultaneously in nearly equal mass proportions at low to moderate pressure (< 5 kb) (Grove & Baker, 1984). The calc-alkaline trend is enhanced by an early crystallization of Mg-rich clinopyroxene and Ca-rich plagioclase at more elevated pressure (> 8-10 kb) in the near absence of olivine (Ghiorso & Sack, 1995; Villiger et al, 2007; Whitaker et al., 2007). Separation of the basaltic andesite liquid into shallow level magma chambers and continued fractionation of Ca-Fe-Mg pyroxene (*cpx*) and Na-Ca-plagioclase produce dacitic to rhyolitic magmas (Figure 10 and 12 SI**)**. Decreasing the magnesium and calcium content in the residual melt promotes the formation of low-Ca pyroxenes that crystallize in the orthorhombic system (i.e. orthopyroxene, *opx*). Importantly, this calc-alkaline trend predicts and explains the chemical and thermal evolution of *cpx*, *opx* and plagioclase reported in **Fig. 2b,c** in the main text. Pyroxene and plagioclase follow consistent trends from ~225 Myr to present, marked by the increasing fractionation of their high-pressure components (i.e. Ca-rich plagioclase and Ca-Mg rich *cpx*) that will deplete the residual melts in Ca and Mg. The marked increase of Ca-poor plagioclase after ~175 Myr is consistent with the sudden occurrence of low-Ca *opx* in the continental magma record. The deepening of the

magmatic chambers where early *cpx* and plagioclase evolve, triggered by a secular cooling of the continental lithosphere and/or its rehydration, could potentially explain this remarkably consistent trend.

Accordingly, Ti-Tschermak substitution in magmatic amphibole also appears to be sensitive to temperature variations (Figure 6 and 7 SI**)** and fluid availability in the continental lithosphere. This leads to the interpretation that Ti-enriched compositions of amphibole crystals form at greater temperatures (Ridolfi & Renzulli, 2012), within hydrated magma chambers (depth < 30 km). The role of Ti in the biotite structure remains uncertain since it may be replacing Si in tetrahedral, or (Fe, Mg) in the octahedral sites (Figure 8 SI). Nevertheless, from the composition of biotites we can gather information about the source of granitoid melts forming or evolving in the upper crustal segments of continents (Shabani et al., 2003). The Mg, Si rich and Al-poor biotite likely crystallized from I-type, mantle-derived magma, where the role of the Al is limited (**Fig. 2d** in the main text). The Fe, Al-rich, Si-poor biotite crystallized from peraluminous melts originating mostly from the partially melted Al-rich continental crust (S-type granitoids), which points to a low mantle-derived magma contribution and/or an elevated rate of crustal reworking at that time. These biotites contain larger amounts of Al_{4+} and low Si in the tetrahedral site and the residual melt is relatively enriched in Si.

II. Extended Method Section

SECTION 1 - Database & statistical approach

The pioneering work of Keller & Schoene (2012) inspired us to compile an extensive geochemical data set of continental and oceanic igneous rocks and minerals from the Phanerozoic to Archaean (Figure 1 SI). Data from the GEOROC database (https//www.georoc.mpch-mainz.gwdg.de/georoc/) were filtered to exclude all samples whose summed oxides yield totals outside the 95-101.5% range. Geochronological data associated with these samples were reported as means with 1-standard-error uncertainty given by the method (e.g.. U/Pb geochronology or biostratigraphy). Geo-referenced bulk-rock chemistry and mineral analysis (3646 references) have been crossed to derive P and T estimates. The resulting dataset includes up to 130 variables for each of the >55,000 whole rock samples, and 80 variables for each of the >117,000 mineral analyses for a total of more than 16 million data points. More than 92 % of the samples correspond to volcanic rocks and >98% of the minerals present in our database have been sampled in volcanic rocks. Results for global mean intensive (geochemical) and extensive (*T, Tp*) values with time are reported with associated 1-standard-error of the sample mean at 50 Myr intervals. The standard error of the sample mean, which is the standard deviation divided by the square root of the sample size, gives us an estimate of how far away our sample error might be form the true population mean. Accordingly, the population mean is within 2 times the standard error from the sample mean about 95% of the time. These means were generated by Monte Carlo analysis, using a standard bootstrap resampling approach that is detailed below.

Our approach follows closely that of Keller & Schoene (2012) adding additional information from the original source (italic) where necessary. *(1) a subset of data was randomly selected so that the probability of inclusion in the resampled subset is directly proportional to sample weight; (2) a synthetic data set for each sampled data point was drawn from a Gaussian distribution with a mean equal to the original value of the data point and standard deviation equal to the estimated 1-standard uncertainty of the data point; (3) the resulting data were sorted into* 50-Myr *bins, with a mean and variance calculated for each variable; (4) steps 1–3 were repeated* 1000 times. *A minimum number of samples (threshold of 3) within each* 50-Myr *was fixed to perform or not the steps 1–3. (5) A total mean and standard error of the mean were calculated for each variable in each bin. Results were reported as means with associated* 1-standard-error of the sample mean *for* 50-Myr *intervals between* 0 and 600 Myr.

In contrast to the approach of Keller and Schoene (2012), which attempted *to produce a uniform record by reducing the weight of abundantly sampled time periods or terranes, our sampling* was not *assigned to be inversely dependent on spatial and/or temporal sample density. Similarly, uncertainties surrounding the age of samples were* not *considered in our statistical approach as this standard error is not homogeneous and will depend of the method of dating used.* Age uncertainties are lower than 50 Myr for > 95% of the mafic samples with a mean uncertainty of around 15 Myr. The uncertaintiesare lower than the results of the bootstrap that we reported as means for 50 Myr intervals and, thus, are not likely to change our general conclusions on the chemical evolution of magmas through geological time. It is noteworthy that our Monte Carlo analysis likely

results in a more discontinuous geochemical record compared to the Keller & Schoene (2012) statistical approach that smoothed out stochastic and stepwise transitions; the slopes of any abrupt trends presented in **Figure 1 (main text)** *are therefore* maximum *estimates.* Overall, we assume that the robustness of our statistical approach is strengthened by the negligible occurrence of sampling gaps for magma and mineral record in the database, more specifically between ca. 0-300 Myr.

As contrasting trends can affect contrasting magmatic systems, we have organized our data into three groups, according to the inferred tectonic environment proposed by the authors of data referenced in GEOROC. These three groups are (1) continental margins, (2) intra-continental settings and (3) oceanic domains. The second group encompasses rift volcanism, continental flood basalts (CFB) and intraplate continental volcanism (including syn- to post-orogenic magmatism). The last group encompasses MORB, submarine ridges, ocean-basin flood basalts (OBFB), ocean island basalts (OIB), oceanic plateaus (OP) and seamounts.

SECTION 2 - Thermometers and barometers for magmatic systems

The chemical record of silicate minerals with extreme geochemical heterogeneities in magma can bring fundamental information on the temperature and depth of magma extraction and evolution in the upper mantle. In this paper, we aim to explore the T and P record of these magmas through a large number of conventional thermo-barometric methods and magmatic minerals such as **olivine**, **pyroxene, amphibole** and **feldspar**. The sequence of crystallization for these minerals is given by the Bowen's Reaction Series, which describes the formation of magmas from different starting T, depth (P) and melt composition.

In tholeiitic magmatic systems evolving at shallow levels in the crust, the sequence of crystallization for magmatic minerals (i.e. the Bowen's Reaction Series) and their compositions depend mainly on the composition of the parental magma and its temperature (Putirka, 2008). Feldspars form a continuous series, evolving from calcium to sodium-rich term as the *P* and *T* decrease. Conversely, Fe-Mg magmatic minerals form a discontinuous series in which olivine stabilizes early, followed by the growth of pyroxene then amphibole and biotite if water is available in the magma. The Mg-Fe substitutions in olivine and pyroxene are *T*-sensitive, Mg-rich endmembers stabilizing at higher temperature in more Mg-rich magmas (Figure 9 and 14 SI**)**. It is noteworthy that basaltic melts evolving in deeper magmatic sources, in often the presence of fluids (e.g. calc-alkaline magmatic systems), are characterized by a different crystallization sequence, with plagioclase, clinopyroxene (*cpx*) and olivine crystallizing simultaneously in near equal mass proportions at low to moderate pressure (< 5 kb) (Grove & Baker, 1984). The calc-alkaline trend is enhanced by early crystallization of Mg-rich clinopyroxene and Ca-rich plagioclase at more elevated pressure (> 8-10 kb) in the near absence of olivine (Ghiorso & Sack, 1995; Villiger et al, 2007; Whitaker et al., 2007). Separation of the basaltic andesite liquid into shallow level magma chambers and continued fractionation of Ca-Fe-Mg pyroxene (*cpx*) and Na-Ca-plagioclase produce dacitic to rhyolitic magmas (Figure 10 and 12 SI**)**. Decreasing the magnesium and calcium content in the residual melt promotes the formation of low-Ca pyroxenes that crystallize in the orthorhombic system (i.e. orthopyroxene, *opx*).

Structural formulae of minerals were calculated using the Excel programs of Tindle & Webb (1994) for amphibole and Putirka (2008) for olivine, pyroxene and plagioclase.

2.1. Thermometry calculations:

Following the methods of Putirka (2008), which were built on a comprehensive review of existing thermo-barometer calibrations for volcanic and intrusive rocks, we compared different magmatic mineral compositions with bulk rock compositions using experimentally derived equations to obtain values for the temperature at the time of mineral crystallization (Figure 2 SI). A large set of P and T values is included in the database. These values were calculated using different equations, the accuracy and range of applicability of which is discussed in Putirka (2008). We selected the most robust equations to unravel the thermal evolution of magma through the Earth's history. Bearing in mind that T and P estimates for samples with significant volatile contents, typical of arc-setting magma, are less accurate, the reported standard error of the estimates (SEE) for hydrous samples is larger. For instance, SEE for the clinopyroxene calibration of Putirka (Equation 32a) increased from ±58°C for anhydrous samples using to ±87°C for hydrous samples.

Olivine-liquid calculations (Figure 3 SI) were performed following Equation (19) and (22) providing the best estimates for anhydrous and hydrous conditions, respectively. Putirka (2008) suggests that difference of temperature between the two equations reflects calibration errors and that there is no disadvantage to using both equations and averaging the results. The accuracy of the averaged calculated temperatures is ±48°C.

Plagioclase *and* ***alkali feldspar-liquid*** (Figure 4 SI) calculations were performed following Equation (24a) and (24b), respectively. They provide the best estimates for anhydrous and hydrous condition. The plagioclase-liquid thermometer is calibrated at T < 1450°C, with a calibration error of ±36°C. The alkali feldspar-liquid thermometer is calibrated at T >1050°C, with a calibration error of ±23°C.

Clinopyroxene-liquid (Figure 5 SI) calculations use Equation (33) calibrated against experiments at pressures less than 70 Kbar to produce a SEE of 45°C. For ***orthopyroxene-liquid*** thermometry, Equation (28a) rectifies past overestimates for the temperature of hydrous samples and is applicable for samples with temperatures from 750 to1600°C, pressures below 11 GPa, SiO_2 weight percent from 33 to 77%, and H_2O less than 14.2 weight percent. Based on petrography, major element compositions and the calculated temperatures, these assumptions are valid for our set of data.

A chemical correlation can be observed in Figure 5c SI between the most Al-depleted **pyroxenes** (diopside /hedenbergite or enstatite/ferrosilite endmembers), which are characterised by high-Mg and -Fe contents, respectively, and the Al-enriched endmembers characterised by depleted Si contents (calcium-, iron or magnesium-tschermak's molecules) or Na enriched content (Jadeite). The large partial molar volumes for Na and Al oxides in basaltic liquid (Lange and Carmichael 1987) combined with the small partial molar volume of Al-rich pyroxenes result in a relatively large P- dependency for jadeite (Jd), calcium-tschermak (CaTs) or iron- -magnesium-tschermak (FmTs) formation compared to other mineral-liquid equilibria. The volume changes for

the solution of Jd and CaTs into diopside/hedenbergite (DiHd) or FmTs into enstatite/ferrosilite (EnFs) are significantly smaller. These exchange-equilibria are temperature-dependent and are calibrated as thermometer for clinopyroxenes and orthopyroxenes, respectively.

2.2. Barometry calculations :

While it is broadly acknowledged that T can be confidently calculated from any silicate mineral in equilibrium with its hosting magma, estimating P using mineral-liquid baromometers is less certain.

Experimentally derived equations to obtain pressure from magmatic mineral are associated with an elevated standard error of the estimate (SEE). The reported SEE is ± 1.5 kbar for the clinopyroxene-liquid barometer (Figure 5d SI) of Putirka (2008) that used a global regression of water-saturated clinopyroxene experiments for calibration (Equation 31). The orthopyroxene-liquid barometer in Equation (29a) provides more accurate pressures for hydrous data but it tends to underestimate low pressures. The maximum inaccuracy is given by the plagioclase-liquid barometer that yield SEE of ± 2.47 kbars.

2.3. Reliability of P and T calculations

Tests for equilibrium between mineral (min) and a nominal coexisting liquid (liq) can be made by comparing observed and predicted values for Fe-Mg exchange, or $K_D(Fe\text{-}Mg)^{min\text{-}liq}$. Analyses that are not within one standard deviation of the equilibrium lines (blue lines in Figure 2 SI) based on the partition coefficient of 0.27 ± 0.03 for clinopyroxene and 0.29 ± 0.06 for orthopyroxene and 0.30 ± 0.03 for olivine were not included in the thermo-barometry calculations (grey points in Figure 2 SI). For plagioclase feldspars, we used a test for equilibrium by comparing An-Ab exchange. The equilibrium constant is not precisely constant, but remains sensitive to T. At T < 1050°C, the value should be about 0.1 ± 0.05, otherwise, it should be 0.27 ± 0.11. Similarly, analyses whose summed oxides yield totals outside the 98.5-101.5% range for these minerals were not included in the calculations.

2.4. Amphibole thermo-barometry

Magmatic amphiboles are considered to represent either (i) primary minerals formed after relatively low-T melting of a hydrous mantle above a dehydrating subducting slab, or (ii) secondary phases formed after crystallization of evolved hydrous silicate melts (Tribuzio et al. 2014) often exsolved from magmas upon crystallization (Coogan et al. 2001; Smith, 2014). Uncertainties surrounding the genesis of magmatic amphiboles have stimulated many experimental studies (Allen and Boettcher, 1983; Sisson and Grove, 1993; Wallace, 2005; Larocque & Canil, 2010) and there is now general agreement that changes in temperature (Ti- and Al-tschermak exchanges : Hammarstrom & Zen, 1986; Hollister et al., 1987; Johnson & Rutherford, 1989; Schmidt, 1992;

Anderson & Smith, 1995; Anderson et al., 2008) and magma compositions (Sisson & Grove, 1993; Pichavant et al., 2002) will affect the composition of magmatic amphiboles.

The origin of high-Si (then low-Al and Ti; Putirka, 2016) amphiboles is classically interpreted as forming in a shallow magmatic reservoir made of evolved (felsic) melts (Grove et al., 2003). This magmatic reservoir can be injected by hot and less-evolved (mafic) melts coming from deeper magmatic reservoirs, resulting in a mixing of magmas (e.g. Humphreys et al., 2009). Mafic melts will form a new generation of low-Si amphiboles in the shallow magmatic reservoir, destabilizing the early generation of high-Si amphiboles (Erdmann et al., 2014 ; Kiss et al., 2014). The intrinsic sensitivity of amphibole to temperature and melt composition, rather than pressure (Putirka, 2016), make the usage of natural amphibole for geobarometry rather controversial if a carefully check for equilibrium textures (i.e. homogeneous composition or normal zonings) is omitted (Ague, 1997; Manley and Bacon,2000; Lindsay et al., 2001; Bachman et al., 2002; Janousek et al., 2004; Blundy et al., 2006; Zhang et al., 2006;, Rodriguez et al.,2007; Anderson et al. 2008; Needy et al.,2009; Samaniego et al., 2008; Ruprecht and Bachmann, 2010; Turnbull et al., 2010). Nonetheless, its potential as a geothermometer is generally accepted (Bachmann & Dungan, 2002; Shane & Smith, 2013).

In this study, we use a new Al-based coupled thermo-barometer model (Ridolfi & Renzulli, 2012), built on an extensive review of experimental and igneous amphiboles. This model yields temperature estimates that are strongly consistent (Yücel et al, 2013, Kent, 2014, Erdmann et al.,2014) with the robust amphibole-plagioclase thermometers of Holland & Blundy (1994) and Blundy & Holland (1990). However, whether the RR2012 method provides a robust barometer remains a controversial issue (Kiss et al., 2014; Erdmann et al., 2014 : Figure 6 and 7 SI).

Chemical data collected on magmatic amphiboles were filtered on the base of pressure-related “apparent percentage error” (APE) values calculated with the RR2012 thermo-barometric method. Following the recommendation of the authors, a maximum of 50 for the APE was imposed to retain or exclude the data (1st filter: moderate confidence level). To secure our estimates, a 2nd filter (high-confidence level) was applied, excluding amphiboles whose chemistry did not fit the dedicated range of chemical composition and structural formulae. More than 70 % of the calcic-amphiboles in our database were discarded.

2.5. Biotite thermo-barometry:

The composition of magmatic biotites (s.l.) present in our database fall within the field outlined by four end-members, phlogopite, annite, eastonite and siderophyllite (Figure 8 SI). In biotite, when compared with phlogopite, magnesium is replaced by ferrous iron and also trivalent ions (Fe3+, Al), and aluminium replaces silicon in tetrahedral sites. Unlike magmatic amphiboles in the calc-alkaline series (Ridolfi & Renzulli, 2012), the role of Ti in the biotite structure remains uncertain since it may be replacing Si in the tetrahedral site, or (Fe,Mg) in the octahedral sites; the later appears more likely given the size of the Ti ion (Deer et al., 2013). Some authors proposed that the partitioning of Ti between magmatic phlogopite and its host rock has an inverse

relation with temperature. It likely decreases with increasing temperature (Righter & Carmichael, 1996), and should not be sensitive to pressure or O2 fugacity variation. Conversely, a positive relationship with temperature has been proposed by other authors for the partitioning of Ti between metamorphic biotite (s.*l.*) and the host rock.

With regard to the dual role of Ti ions, we preferred the use of aluminium content in biotite (s.l.) as a proxy for unravelling the thermal regime of biotite-bearing magmas forming or evolving in the upper-crustal sections of the continental lithosphere (Buda et al., 2004). Accordingly, it is thought that minerals formed at higher temperatures in mantle-derived magmas (I-type granitoids) tend to have less Al in four-fold coordination (Al4+) compared to those formed after crustal reworking/melting (S-type granitoids).

SECTION 3 - Unravelling potential temperature (Tp) of the upper mantle

The potential temperature (Tp) of the upper mantle, which is the temperature that the solid adiabatically convecting mantle would attain if it could reach the surface without melting, reflects a balance between heat gain by radioactive decay in the mantle and heat loss by convection and surface diffusion. How this balance has varied over geological time is still under discussion in the light of geophysical modelling of the thermal state of the Earth (Anderson, 2000 ; Korenaga, 2006 ; Labrosse & Jaupart, 2007 ; Davis, 2009). Recovering this information through geochemical modelling is more straightforward. It relies on the chemical record of particular igneous lava (primary magmas, Herzberg & Asimow, 2008 ; Putirka, 2008) that may have formed by melting of dry and fertile peridotite and that underwent limited differentiation (fractional crystallization) before magma emplacement in the crust.

Volcanic activity along mid-ocean ridges and continental rifts gives birth to primary magmas through decompression melting of the shallow sub-lithospheric mantle, or the so-called ambient mantle. Inferences, though limited, already provide fundamental information about the thermal state of this ambient mantle as a function of time (Herzberg et al., 2010). In contrast, intraplate volcanism, which also gives birth to primary magmas through decompression melting of deep, hot mantle (Herzberg & Gazel, 2009) or decompression melting of warmed ambient mantle (Grigné et al., 2005) beneath thick lithospheric keels (Bédard, 2006; Ernst, 2009), has been poorly investigated in the Palaeozoic record. Acknowledging that > 85% of the present-days thermal anomalies giving birth to intraplate magmatism could have formed in the upper mantle (Courtillot et al., 2003; Husson & Conrad, 2012), there is an intriguing interest to integrate this complementary set of primary magmas values when discussing the thermal regime of the upper mantle, not only the ambient mantle (Herzberg et al., 2010), as a function of time (Anderson, 2000).

3.1. Liquid thermometry

We obtained primary magma (lava) compositions and mantle Tp values using the ***PRIMELT3 MEGA*** software (Herzberg & Asimow, 2015). The software is calibrated by anhydrous melting experiments on fertile peridotite, and its application to lavas assumes a similar fertile and dry peridotite source. Uncertainties in fertile peridotite composition do not propagate to significant errors in mantle Tp (Herzberg & Asimow, 2008). Conversely, melting of wet peridotite is likely to propagate to MgO and mantle TP that are too elevated. We discuss this point below. PRIMELT software provides solutions for both batch and accumulated fractional melting, and we use the results for the latter. PRIMELT automatically filters and excludes all samples that have undergone augite and/or plagioclase fractionation as indicated by depletion of CaO and Al_2O_3. Our solutions of calculation have been filtered according to a graphic procedure (Herzberg & Asimow, 2008), reducing uncertainty arising from pyroxenite source lithology, source volatile content from metasomatized peridotite, and clinopyroxene fractionation. The remaining samples (271) were assumed to have been affected only by variable amounts of olivine addition and subtraction.

Mantle Tp calculation using PRIMELT is inferred from the MgO content of the primary magma, whereby MgO typically correlates with FeO. The calculations require that FeO be obtained from FeO_T . estimated assuming Fe_2O_3/TiO_2 = 0.5 in Figure 15 SI. Melting is assumed to have been fractional, not batch, and all calculated primary magma compositions are aggregates of all melt increments that mix perfectly. Solutions of our calculations (271 data) are provided in the supplementary material (Table 1 SI). A more oxidizing ratio of Fe_2O_3/TiO_2 = 1, suitable for some arc-related basalts (Herzberg & Asimow, 2008), will likely decrease FeO in the primary magma, yielding lower MgO and lower mantle Tp (Herzberg & Gazel, 2009). We tested this hypothesis and results are given in Figure 16 SI. The 0.5–1.0 range in Fe_2O_3/TiO_2 propagates to Fe^{2+}/Fe_T values that vary from 0.76 to 0.99 for the set of data used in this study. Accordingly, uncertainties in Fe_{2+}/Fe_T propagate to uncertainties in mantle Tp lower than 30 °C for low-Ti type lavas (TiO_2<1 wt% ; common) and up to 80°C for high-Ti types (TiO_2>2.5 wt% ; unusual). As a whole, our adoption of a more reduced Fe_2O_3/TiO_2 value will likely provide a maximum estimate of mantle Tp.

3.2. Results

Tp minima in the Cenozoic record (<65 Myrs) is largely derived from primary magmas formed in arc setting or along accretionary ridges. The Siqueiros Fracture Zone of the East Pacific Rise (EPR) is the only present-day MOR (mid-oceanic ridge) that provides successful solutions of calculation at around 1350°C with PRIMELT. All other primary magmas appear too differentiated (Herzberg & Asimow, 2015). There is, thus, no inconsistency in the Tp minima record of our dataset, where the expected 1350°C values are missing (caption a). Thermal anomalies, from which the “hot” primary magmas are derived (Tp maxima in Figure 16 SI), are likely to be produced by deep mantle upwelling, which originates from instabilities in a thermal boundary layer. The most likely location of such a boundary layer is at the transition zone (410 - 660 Km). An adiabatic temperature increase of ~200 °C has been proposed through the first 400 Km off the upper mantle (Katsura et al, 2010), which is consistent with the difference of temperature (Δ Tp ~200°C) depicted by the primary magma compositions. It is noteworthy that Δ Tp remains broadly constant throughout the Earth history (i.e. ~200°C) and we suggest that Tp values calculated in the Precambrian times can also be representative of vertical temperature

changes in the upper mantle at that time, from a shallow ambient mantle (Tp minima) to a lower thermal boundary layer (Tp maxima). A limited decrease of ~100°C is thus proposed for Tp minima and Tp maxima since ~2.5 Gyrs.

Likewise, we suggest that insulation of the upper mantle beneath growing supercontinents (Grigné et al., 2005 ; Coltice et al, 2007 ; Coltice et al., 2009; Farrington et al., 2009 ; Rey, 2015) leads to the generation of mantle plume-like clusters with elevated Tp values, impacting the distribution of temperature gradients in the upper mantle without modifying the secular trend of cooling for Tp minima and maxima. Accordingly, the increase and subsequent decrease of Tp-average before and after ca. ~ 300 Myrs is likely reflecting a general warming then cooling of the sub-continental mantle (SCM) accompanying the formation and disassembly of the Pangea supercontinent (Figure 17 SI). Insulation of the Archaean mantle beneath a growing supercraton or large stagnant plate (Ernst, 2009) could explain the cluster of Tp values positioned at elevated temperature around 2.5-2.8 Gyrs, assuming that the geochemical data set collated for the Archaean terranes (i.e. greenstones) mainly corresponds to a continental igneous rock record.

3.3. Assumptions on water and redox conditions in the source using PRIMELT

In this paper, we discuss the importance of anhydrous fractionation (pyroxene) through the SCLM and hydrous fractionation (amphibole) in subduction zone magmas leading to the observed differences between average primary and mafic magma compositions. It is worth noting that melting processes in arc-settings or large igneous provinces (LIPS) vary greatly (i.e. flux vs decompression, respectively), however, the primary melt temperature (Tp) calculated by PRIMELT does not depend of the water content in the mantellic source as it assume an anhydrous adiabatic decompression melting. Accordingly, PRIMELT has been calibrated using experiments on anhydrous systems, and was – in theory – not intended to be applied to arc magmas. As outlined above, no pre-selection of data using different trace element ranges was applied, as recommended by Herzberg and coworkers (Herzberg et al., 2010) to distinguish MOR (mid-oceanic ridge) type mantle from plume types of mantle or from arc types of mantle. We acknowledge that disregarding the geological context in which the lavas formed represents the most inherent risk of our “blind” approach as the hydrous and redox states of the mantle source controlling the reliability of our Tp calculations are likely to change with the geological context and we cannot easily account for these changes in our global approach.

In Figure 15a SI we calculated our primary magma composition using a standard procedure for MOR type mantle (Herzberg et al., 2010), assuming reduced conditions in the source. It is generally agreed, however, that subduction zone occurrences, and to a lesser extent LIPS and OIBS (ocean island basalts), are more hydrated; therefore, the effect of using anhydrous melting will lead to a overestimation of mantle potential temperatures for subduction and some plume settings (Herzberg & Asimow, 2008). This point is particularly relevant for the Tp record of young Cenozoic lava in our database for which we can easily infer the geodynamic setting. Many of them come from subduction zone occurrences or from LIPS, OIBS or oceanic plateaus (OPS) (i.e. Emeishan, Wrangellia, Central Atlantic magmatic Province, Karoo, Etendeka, Manihiki plateau, Caribbean Large Igneous Province, Hawaii, and the North Atlantic Igneous Province : see geological map in the supplementary material).

Conversely, inferring the geodynamic setting of oldest magmas in our database, especially those spanning the Palaeozoic times is less easy as it relies heavily on the trace element signatures of magmas (O'Neil et al., 2011), which is somewhat problematic.

As an example, it is widely accepted that the single most distinctive feature of volcanic rocks from convergent margin settings is a marked depletion of the high field strength elements (HFSE) Nb, Ta, and Ti relative to large ion lithophile elements (LILE) and light rare earth elements (REE) when compared with basalts from MOR and OIS (Pearce & Peate, 1995). However, a major impediment to the geochemical geodynamics investigations using old data source in GEOROC is the lack of high-quality data for the HFSE (particularly Nb and Ta) that occur in very low concentrations in most volcanic rocks from convergent-margin settings. Another common problem is the ambiguity surrounding the Na/Ta anomaly that is classically viewed as reflecting the fractionationof amphiboles in the source, inferring the presence of water in the geological setting where magma formed. However, it has been also proposed that Na/Ta anomalies can be better controlled by anhydrous Ti-phases suchas titanite or rutile (Klemme et al., 2002), reflecting different depths of fractional crystallization and/or degrees of melting (John et al., 2011).

We acknowledge there is certainly a real advantage in strengthening our PRIMELT modelling with the use of appropriate redox values for the youngest magmas formed in well-constrained geological settings; however, it introduces an increased risk of major selection bias and errant parameters for subsequent calculations. Conversely, there is an intrinsic risk in running PRIMELT with inappropriate redox conditions, but there are also some benefits in performing our calculations with consistent parameters on a complete dataset to obtain qualitative or semi-quantitative information. Accounting for these limitations and methodological assumptions that are mutually exclusive, we consider our approach as meaningful as that as proposed by Herzberg and coworkers (Herzberg et al., 2010).

Nonetheless, to minimize the inherent risk of using PRIMELT on hydrous magmatic systems (which is not recommended), we filtered our PRIMELT solutions for arc settings, accounting for GEOROC information (Figure 16e SI) and excluded data (Figure 16f SI with HFSE Nb/Ta ratio > 17 (Stolz et al., 1996). No significant differences are observed for Tp maxima and minima through times. It will be also argued that PRIMELT solutions for arcs are restricted to the ca. 0–140 Myrs and thus are not likely to change our general conclusions on the thermal regime of the upper mantle through the Phanerozoic times.

We conclude there is little else we can do at present to further test the reliability of our results with PRIMELT other than arguing (1) of the potential constancy of redox conditions in the upper mantle sources, in depth and time (Li & Lee, 2004), that is likely to generate minor uncertainties in our solutions of calculation ; (2) that assumptions about redox conditions will not greatly impact estimates on Tp when working with arc-related magmas, although more oxidized assumptions will lower Tp ; and (3) of the capacity of PRIMELT to identify magmas generated from hydrous arc sources (lavas that lost Ol ± Plag ± Cpx and/or Amph) and/or that have been degassed from CO2-rich sources and to exclude them. It will be also argued that some mafic magmas

forming in arc-settings don't require hydrous conditions for mantle melting and could potentially provide viable magma suites for Tp calculations using PRIMELT.

3.4. Olivine-Liquid thermometry

Whilst it is increasingly accepted that statistical geochemistry can be established as a viable and powerful approach to understanding global issues in Earth Sciences, the robustness of geological interpretations derived from the PRIMELT approach remains in doubt when the secular changes are not sufficiently supported by data. A robust bootstrap analysis requires high data density and temporal continuity in the dataset to ensure data representativeness (Keller & Schoene, 2012). Hence care must now be taken to assess the global significance of the ca. 300 Myrs thermal event recorded by anhydrous primary magmas and its consistency with existing framework of global tectonics using a more comprehensive set of data.

Accordingly, magmatic rocks have been re-analyzed with the olivine- and glass-based thermometers of Putirka (2008) to obtain information on mantle-derived primary magma compositions from a largest range of mantle rocks composition, among which peridotites metasomatized at plate margins during Pangea break-up. We carried out the following steps: (1) we estimate melt fraction (F = 0.15 or 0.25) and add an upward T correction on olivine temperatures obtained with the olivine-liquid calculation (see above). Here, T correction, accounting for the heat of fusion, is equal to delta-H*F/Cp, where delta-H is about 100 kJ/mole and Cp = 200 J/K; note that delta-H is less than what Putirka published in 2005 and 2007, but the author considers (personal communication) this lower estimate as more appropriate as an all-around value; (2) we estimate melting depth for each parental magma and decrease T by 1.3°C/GPa. There are simple equations in Putirka et al. (2007) to estimate F, and both Lee et al. (2009) and Putirka (2008) provide Si activity models to estimate depth.

More than 5,600 successful Tp solutions have been obtained for a total of > 14,300 olivine-bearing samples (Figure 17 SI).

3.5. Epilogue : what is a "mean" in Petrology ?

Sampling is the basis of all works in Earth Sciences, so diverse they are. In petrology, the sample on which we base our thinking is seen as part of a whole, chosen to represent one or more characteristic properties of that set. But is it really the case?

All sampling, even the simplest, is subject to several sources of error related to the sampling technique, how we apply this particular technique, or to the instrument of sampling. When the volume of the sample is too large, it must be down sampled to only analyze a small portion of the sample. The risk of selecting the most spectacular sub-sample, distorting the representation of this set, is omnipresent. Each step of down sampling implies an error and these errors accumulate, altering our perception of an event or a geological process. Geostatistics can help quantifying the magnitude of these errors but requests to work on quite big datasets to extract an average value

("mean"). The estimated mean of a variable is only possible if we measured this variable on a large number of samples. Thus the quantity and quality of sampling does influence that of the "mean" itself. There is no need to develop sophisticated estimation techniques if the database is not reliable. The multi-scale processing of these data is a relatively recent approach in Earth Sciences, arising from the need to take into account all phenomena, in practice coupled, that have acted on (or are present in) a given system. This is the most complete form of modeling of a sequence of various phenomena proceeding at different orders of magnitude, since it integrates, at different scales, all theoretical or empirical knowledge in elementary bricks that need to be assembled. Here, we opted for this integrated approach, emphasizing that our conclusions can only provide insight into dominant large-scale trends.

Recent advances in the domain of igneous petrology (Ghiorso & Sack, 1995; Herzberg & Asimow, 2008 ; Putirka, 2008) occurred along with the development of chemical databases of magmatic rocks and minerals, providing access to several tens of thousands rocks and minerals analyses spanning most of the Earth's history. Data mining techniques allow the exploration of these datasets to uncover hidden patterns and trends over time periods several tens to hundreds of millions of years, matching those of geodynamics (Keller & Schoene, 2012 ; Tang et al., 2016). As they incorporate a growing number of data, the results of these new global studies are surrounded by a statistical dimension out of necessity, which makes them quite unpopular in the scientific community of petrologists. Yet, these new approaches are necessary because they capture the geological signals at longer wavelengths, smoothing the analytical errors, filling the sampling bias and averaging values along secular trends. Accordingly, the "petrological mean" computed from these studies has a real meaning because it fully accounts for (and not masks) the natural variability in petrology that arises from variable temperature (and depth) of partial melting and crystallization in igneous rocks from widely different geological environments (arcs, cratonic provinces, ocean…).

Here, we opted for this integrated approach, emphasizing that our conclusions can only provide dominant trends rather than strict rules. Let's consider the olivine record. Statistically speaking, increasing the number of Mg-rich olivine analyses will force the bootstrapped mean toward a higher value, at a specific step of age considered. The mean of "Tp" depicted from the selective PRIMELT method (Figure 15 SI) reveals elevated temperatures in the Permian times (1525°C) and a lower thermal regime in the recent record (1425°C). Now, if we compare the "mean" of PRIMELT with those derived from the less selective Ol-Liq. approach (that possibly tapped some fractionated basalts from the crust), the absolute values are different (which seems logical because hydrated mantle magmas from arc settings yield lower Tp), but the relative difference (~100°C) is similar (Figure 17 SI. This is part of why we think the ol + cpx + plag chemical trends are also interesting in order to discuss the thermal evolution within the continental lithosphere. This is also the case for the chemical trends of amphibole and biotite evolving in the continental crust. All these minerals trends appear real and we are able to connect these trends to something geological. In this paper, we show that the nature and temperature of magmas extracted from the convective mantle, the lithospheric mantle and the continental crust evolved on a time scale of a few 100's of Myr, capturing the amalgamation of Pangea and its subsequent dispersal.

(B) Supplementary Figures

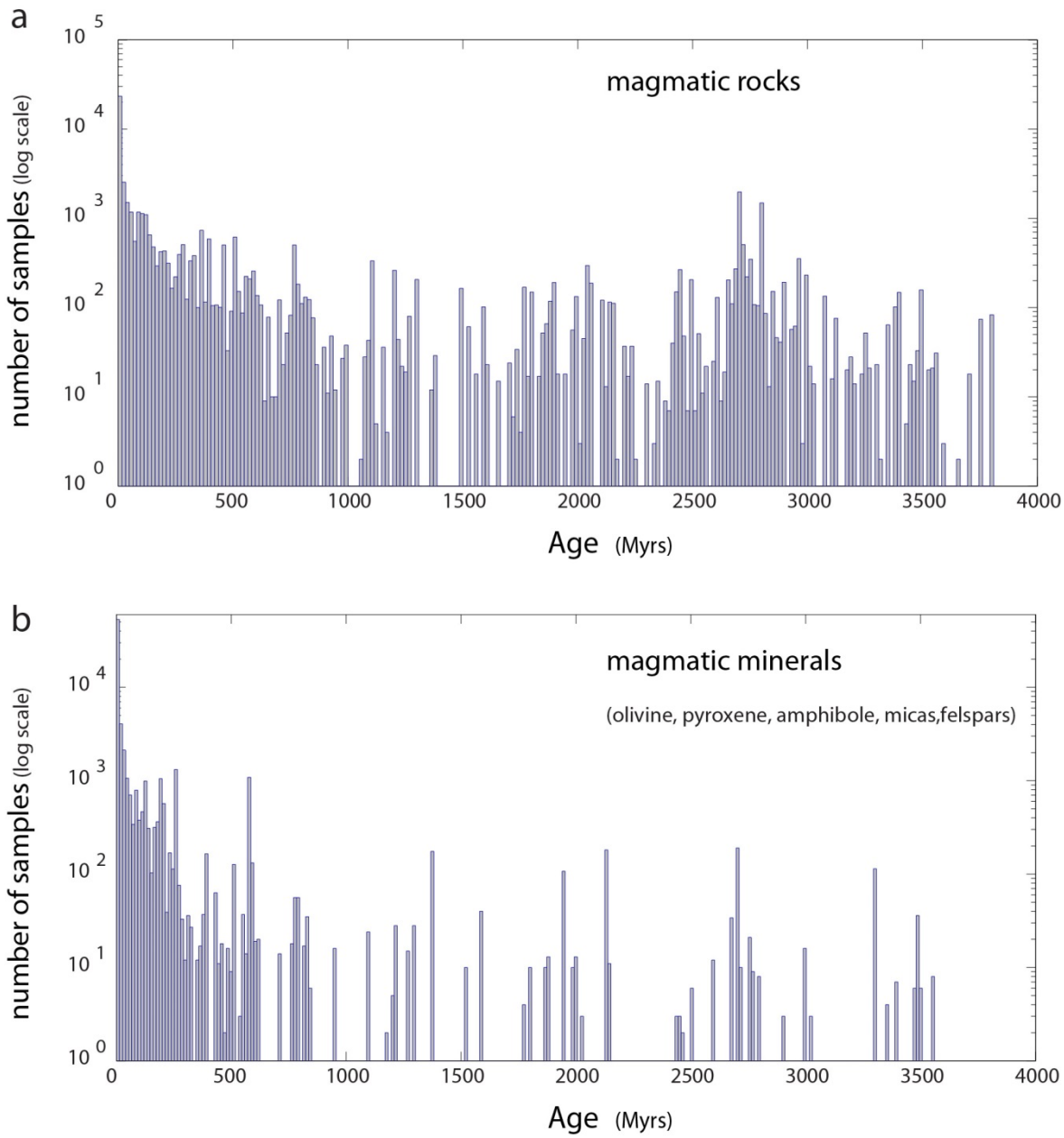

Figure 1 SI. (a) Distribution of magmatic rocks considered in this study (>55,000 samples) plotted again their age. The data illustrates a reasonable distribution of mafic and felsic magmas through the Earth history (source : Georoc). (a) Distribution of magmatic minerals considered in this study (> 117,000 analysis) plotted again their age. An intriguing lack of mineral analysis is observed in the Precambrian times, hampering the use of classic thermometers (Putirka, 2008; Ridolfi & Renzulli, 2012) to investigate the thermal evolution of mafic to felsic magma.

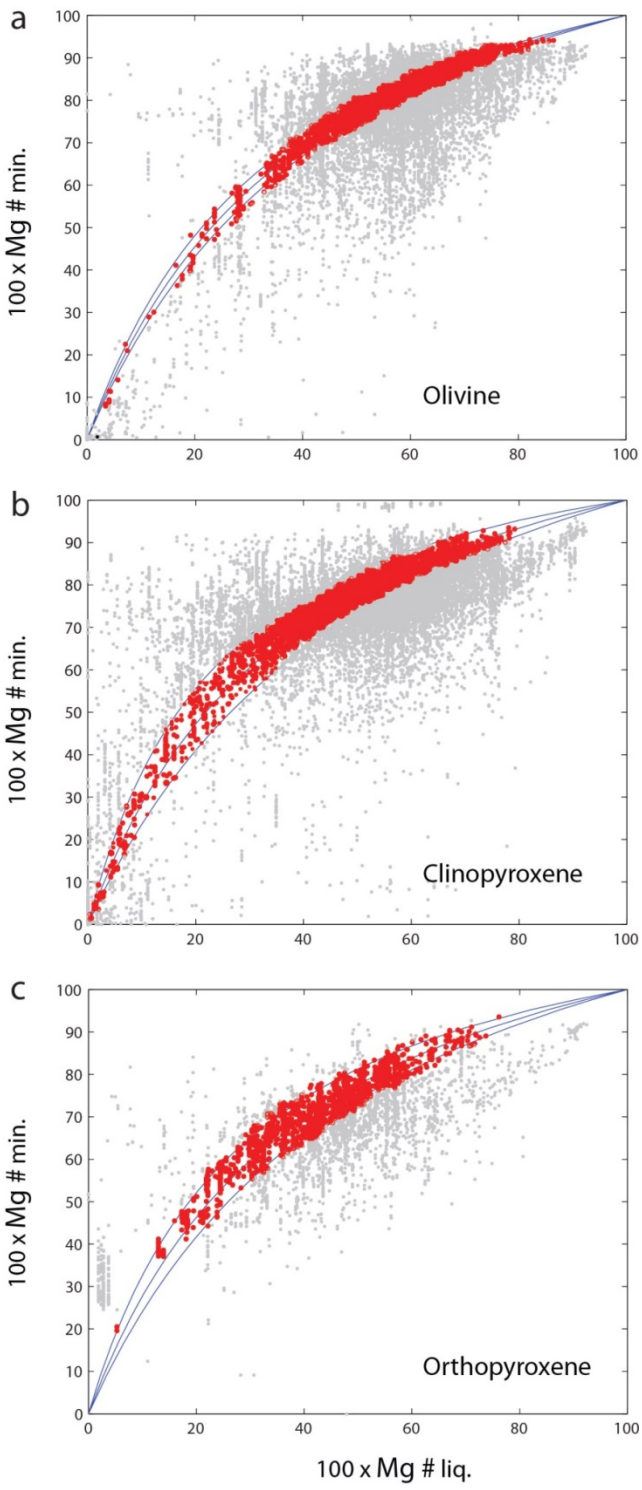

Figure 2 SI. Tests for equilibrium between mineral (min.) and nominal coexisting liquid (liq.) can be made by comparing observed and predicted values for Fe-Mg exchange. Analyses that are not within one standard deviation of the equilibrium lines (red points) based on the partition coefficient [$K_D(Fe\text{-}Mg)^{min\text{-}liq.}$] of 0.27±0.03 for clinopyroxene and 0.29±0.06 for orthopyroxene and 0.30±0.03 for olivine were not included in the thermo-barometry calculations (grey points).

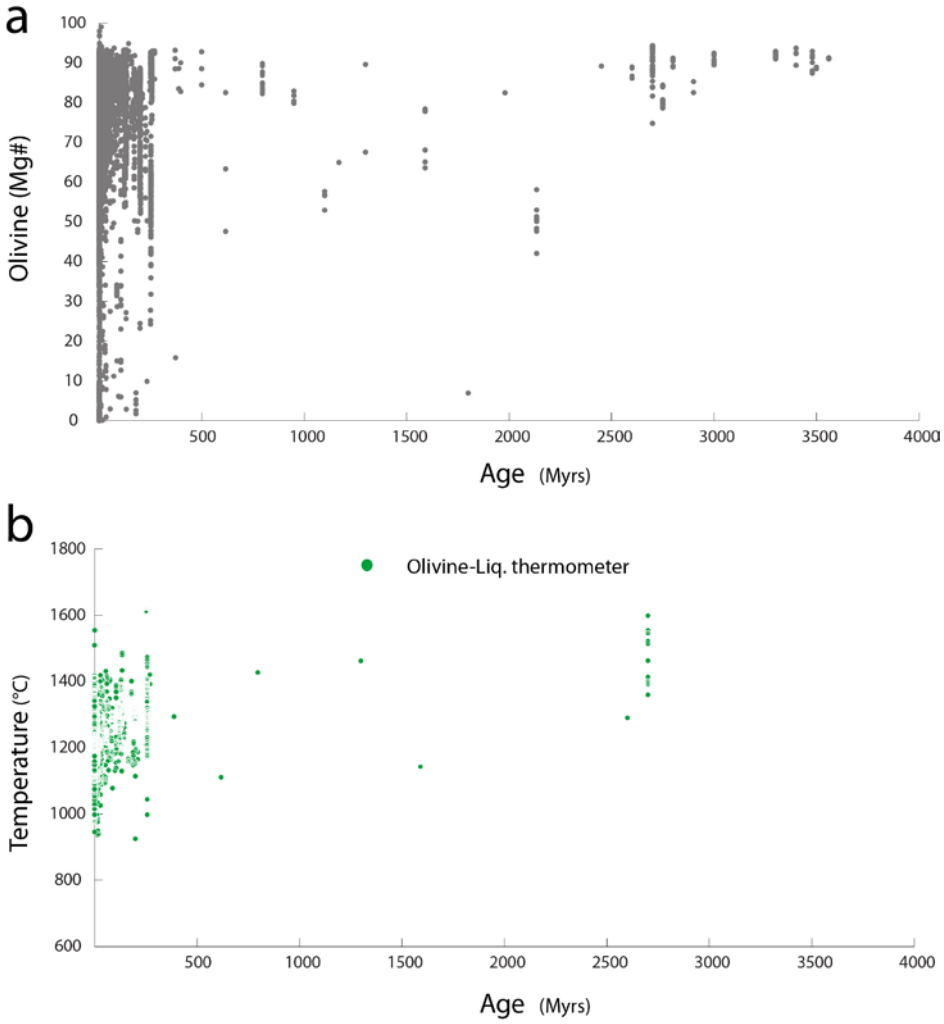

Figure 3 SI. (a) Chemical evolution of olivine (Mg#) according to their age (18,749 analyses). (b) T conditions of olivine crystallization calculated using the Putirka (2008) method (min.-Liq.) vs time (7,206 analyses).

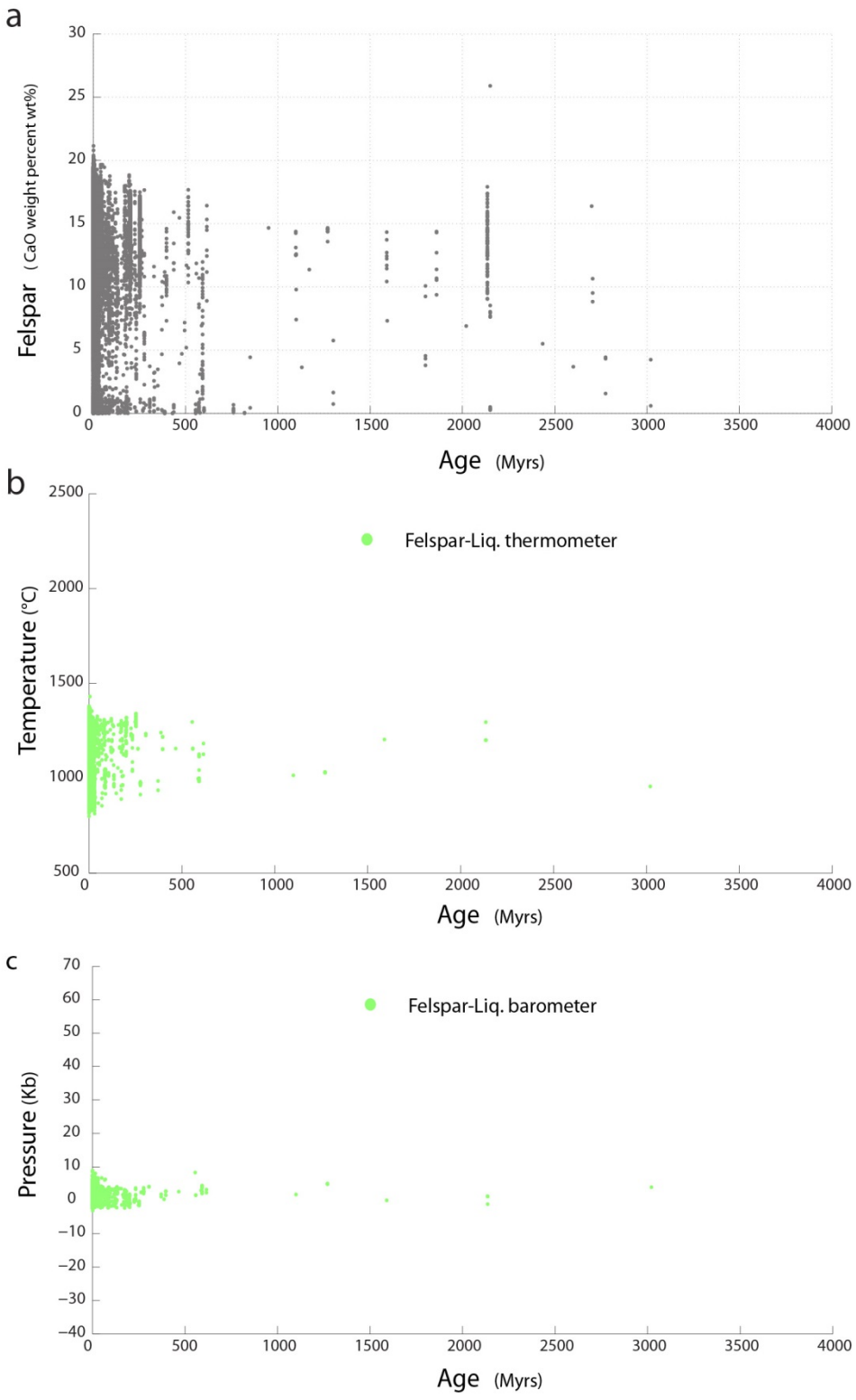

Figure 4 SI. (a) Chemical evolution of feldspar (CaO/CaO+Na_2O wt% ratio) according to their age (23,996 analyses). (b) T conditions of felspar crystallization calculated using the Putirka (2008) method (min.-Liq.) vs time (7,140 analyses).

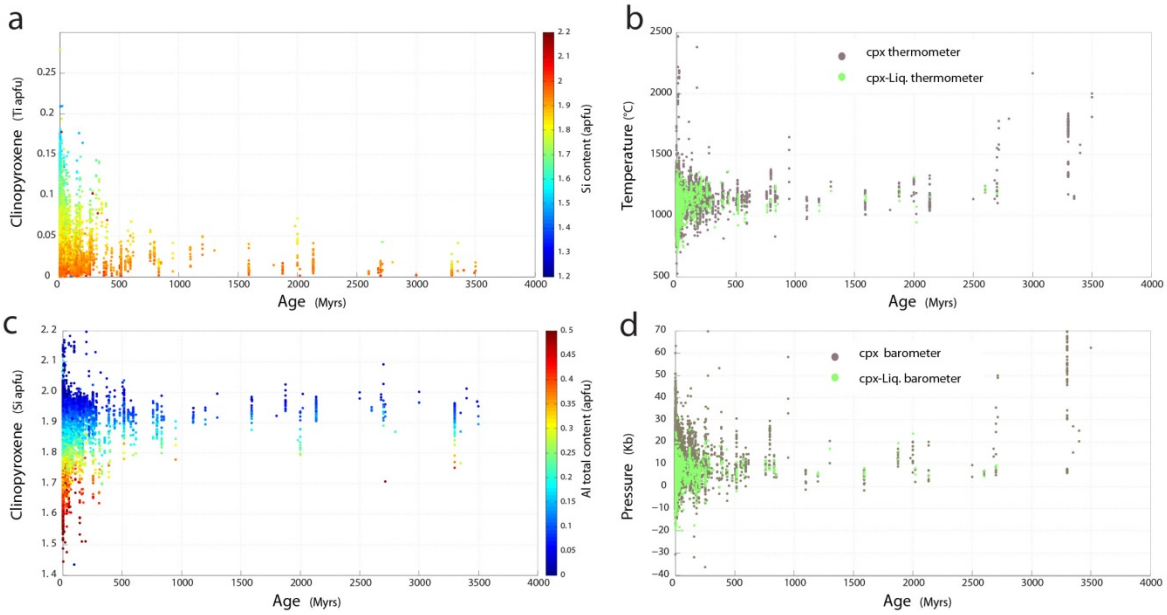

Figure 5 SI. (a, c) Chemical evolution of clinopyroxene (Ti and Si apfu) according to their age (16,683 analyses). (b, d) T and P conditions of clinopyroxene crystallization calculated using the Putirka (2008) methods (min.-Liq : 4,689 analyses; mineral-only :16,683 analyses) vs time.

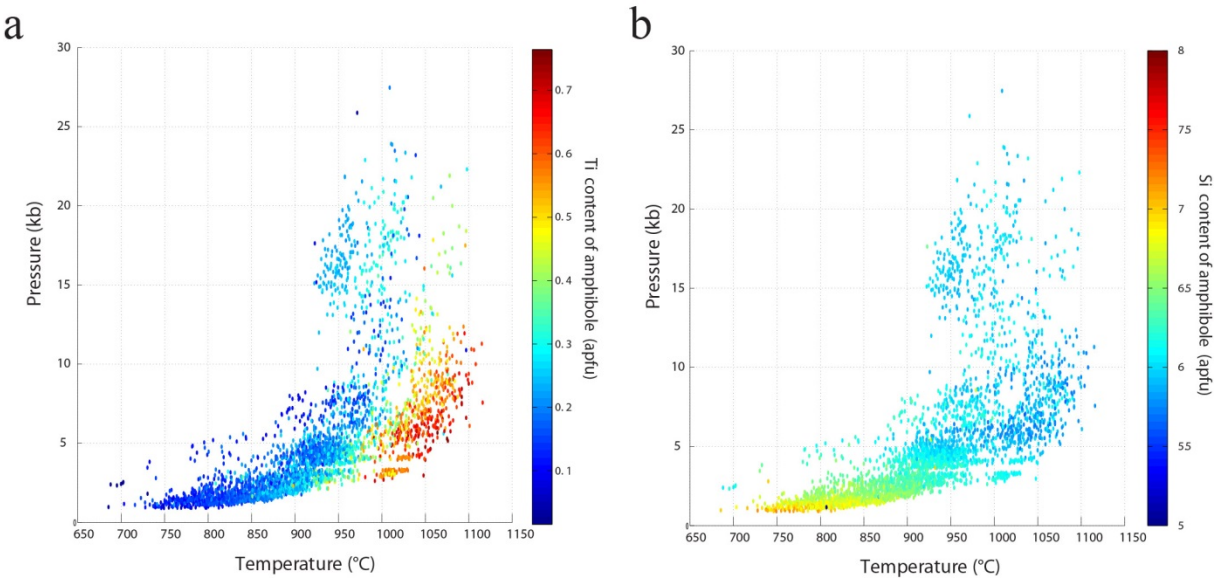

Figure 6 SI. Pressure (P) and Temperature (T) conditions of amphibole crystallisation, calculated with the Ridolfi & Renzulli (2012) (RR2012) method, plotted against their chemical composition (3,551 analyses). (a) Ti (apfu) evolution in amphibole showing the dominant control of temperature on the Ti-tschermak substitution. (b) Si (apfu) evolution in amphibole showing the dominant control of pressure on the Al-tschermak substitution. Data suggest that high-Ti and low-Si amphiboles are stable at higher temperature and pressure.

.

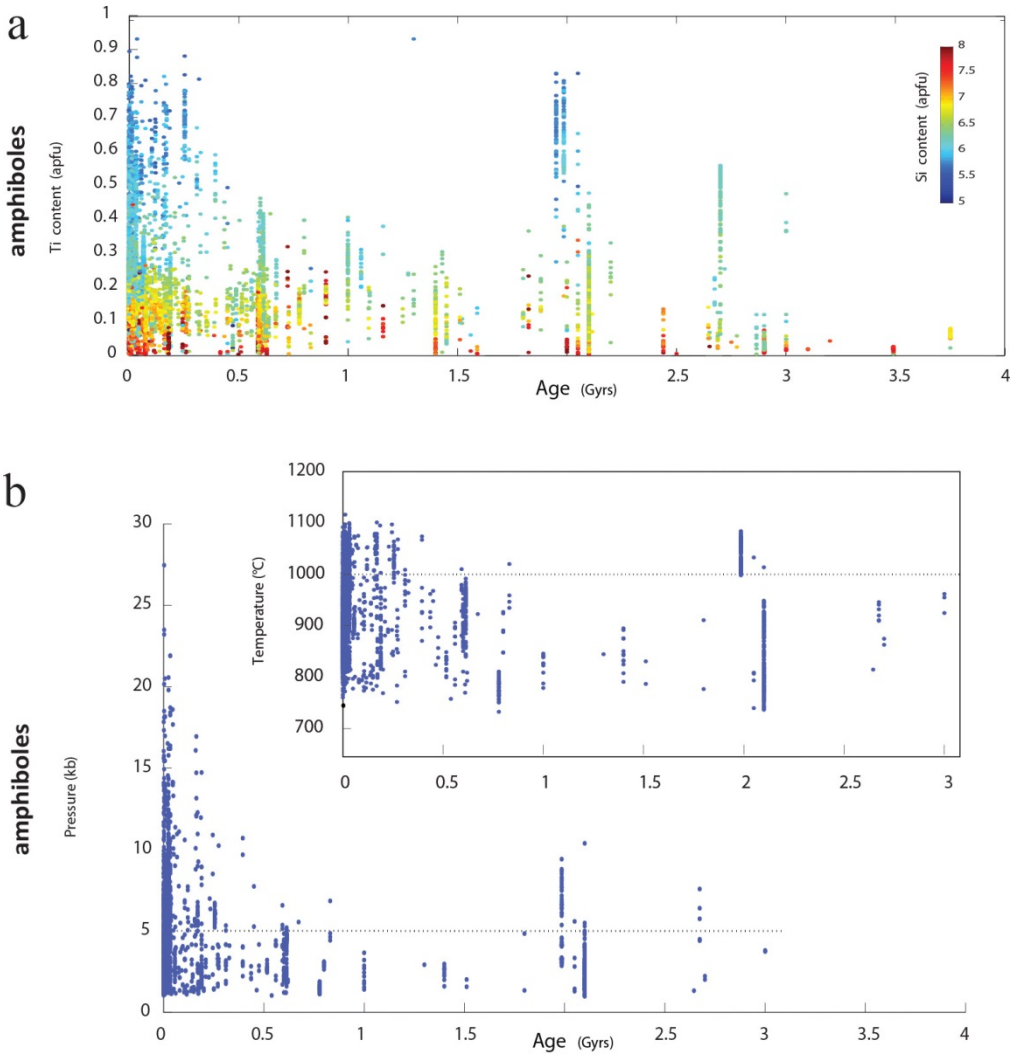

Figure 7 SI. (a) Chemical evolution of amphibole (Ti and Si apfu) according to their age (11,218 analyses). (b) T and P conditions of amphibole crystallization (blue points) calculated using the RR2012 method vs time (3,551 analyses).

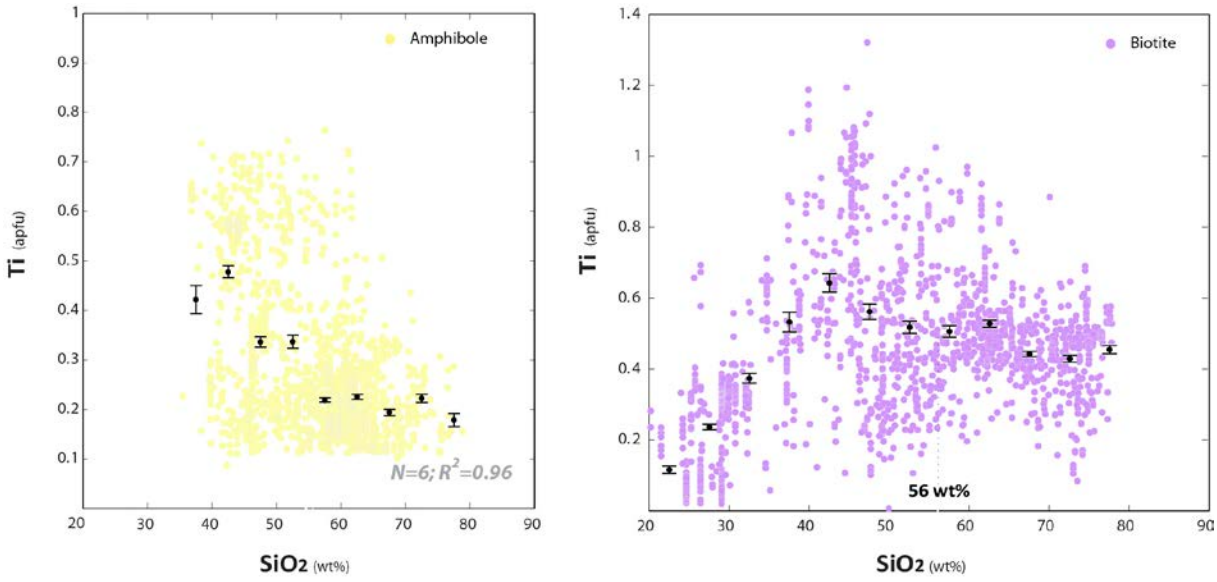

Figure 8 SI: Chemical evolution (Ti apfu content) of biotite (s.l.) and clinoamphibole according to their bulk roch composition (3440 analyses for biotite ; 1767 analyse for amphibole). The division between phlogopites and biotite (s.s.) was arbitrarily chosen to be where Mg : Fe = 2:1. Remarkably, this boundary corresponds to a major change for Ti in biotites (s.l.) that shift from a positive to a negative correlation with the SiO_2 composition of the hosting rock (i.e. Ti-poor, Mg-rich phogopites form in Si undersaturated magma ; Ti-poor, Fe-rich biotites [annite] form in Si saturated magma). Amphibole yielding T estimates using the RR2012 method show a negative correlation with the Si of the magmatic rock.

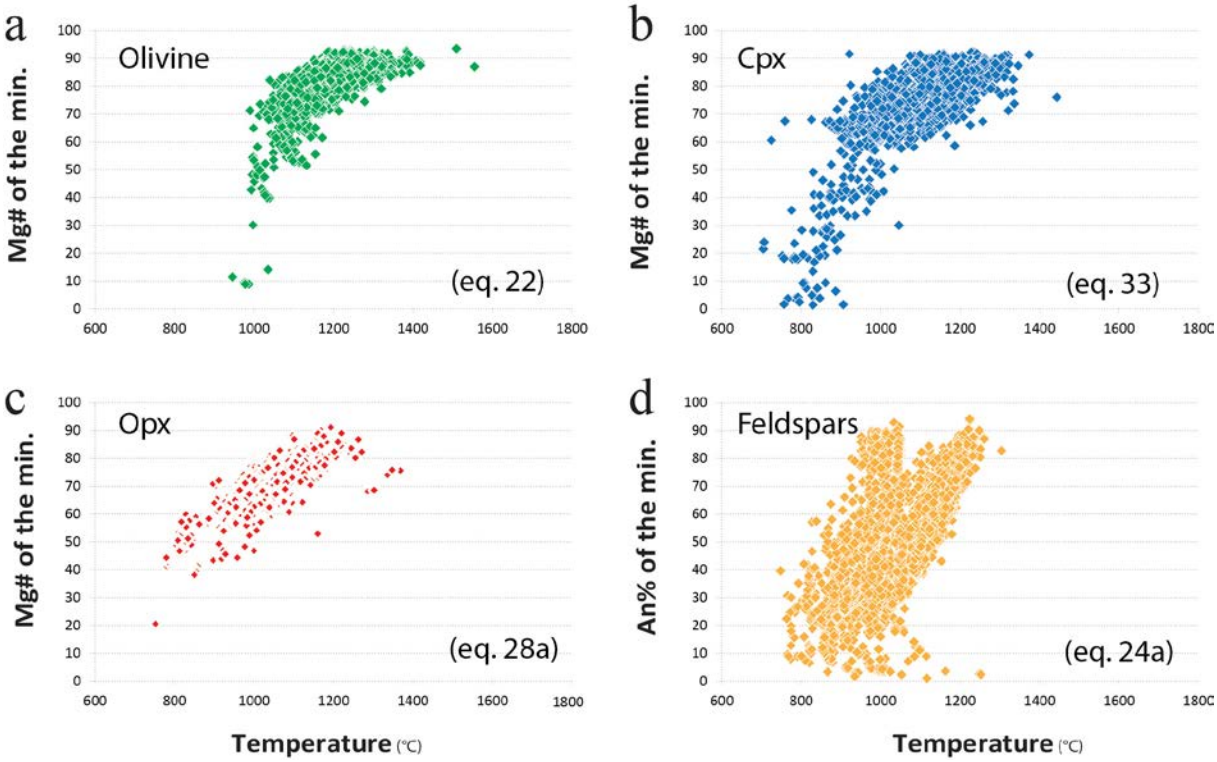

Figure 9 SI. T conditions of magmatic mineral crystallization obtained with different thermometers (Putirka, 2008) and plotted against their chemical composition. Data suggest that high-Mg olivine (a,) and pyroxenes (b, c) are stable at higher temperature. (d) X Anorthite [Ca/(Ca + Na + K) ratio] evolution in felspars showing the dominant control of temperature on the Ca-Na substitution

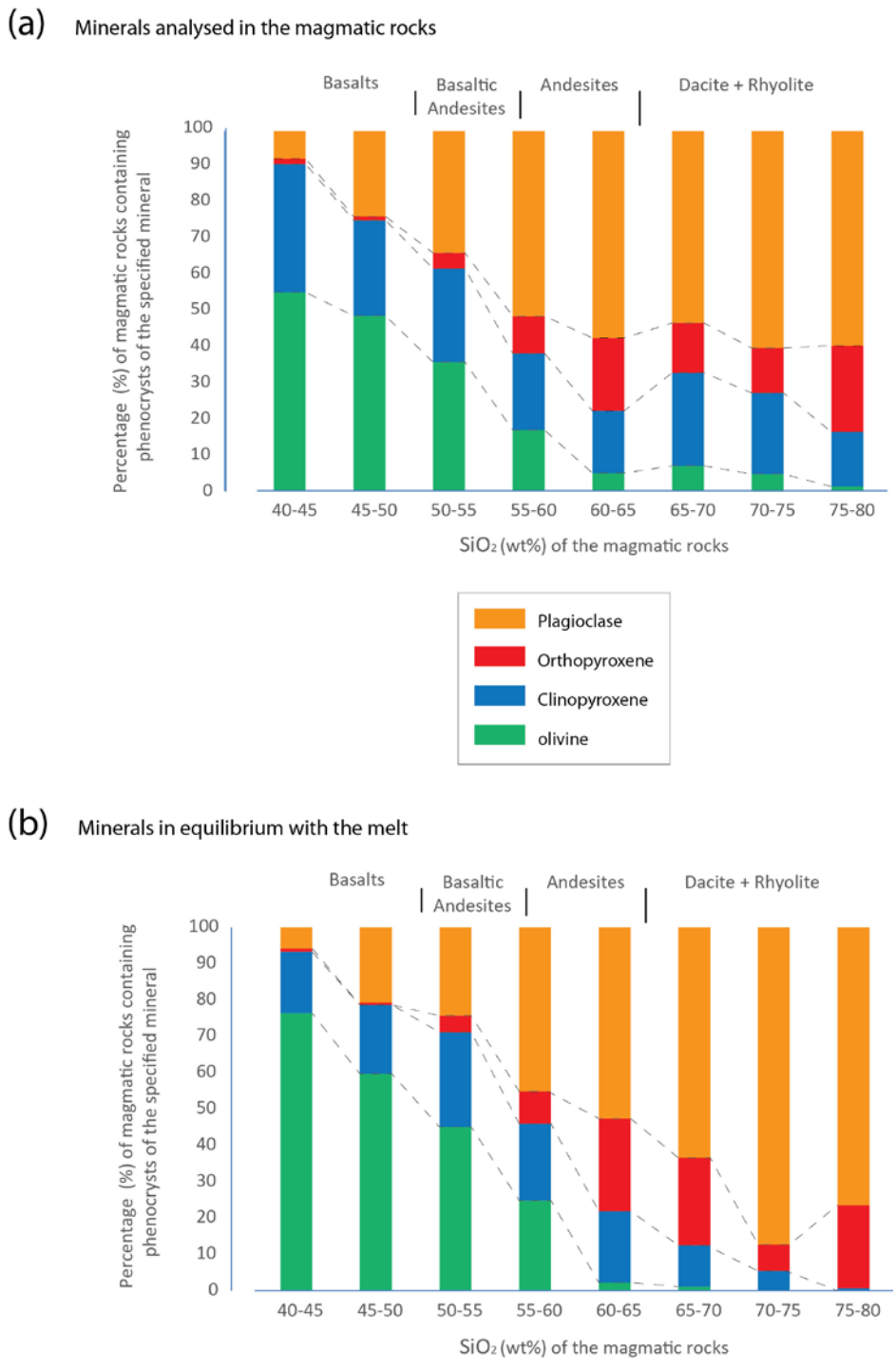

Figure 10 SI. Cumulative histograms for the occurrence of selected magmatic minerals (ol, cpx, opx, pl) as phenocrysts in the continental record. Figure (a) concerns mineral in equilibrium and disequilibrium (residual) with the hosting rock. In (b), only minerals in equilibrium with the magmatic rocks have been considered. Olivine proportion is dominant in Si-poor composition of magma whereas the couple orthopyroxene-plagioclase is dominant in the Si-rich component of magmas. Note that clinopyroxene appears within a wide range of composition in nearly similar proportion.

A statistical treatment of data, using a small step of sampling (25 Myrs, red points), helped to better visualize the increase of peraluminous magmas record at the beginning of the Phanerozoic times (600 to 400 Ma). Note that the ca. 375 black dot was not included in the calculation of the yellow curve. It inconsistency compare to the rest of data could be explained by a bias of sampling in our database, for which the (diamond-rich) kimberlite singularity have pervaded the discussion of Russia and South Africa cratons evolution, resulting in an increasingly number off Al-poor rocks sampling compare to their relative distribution at that time.

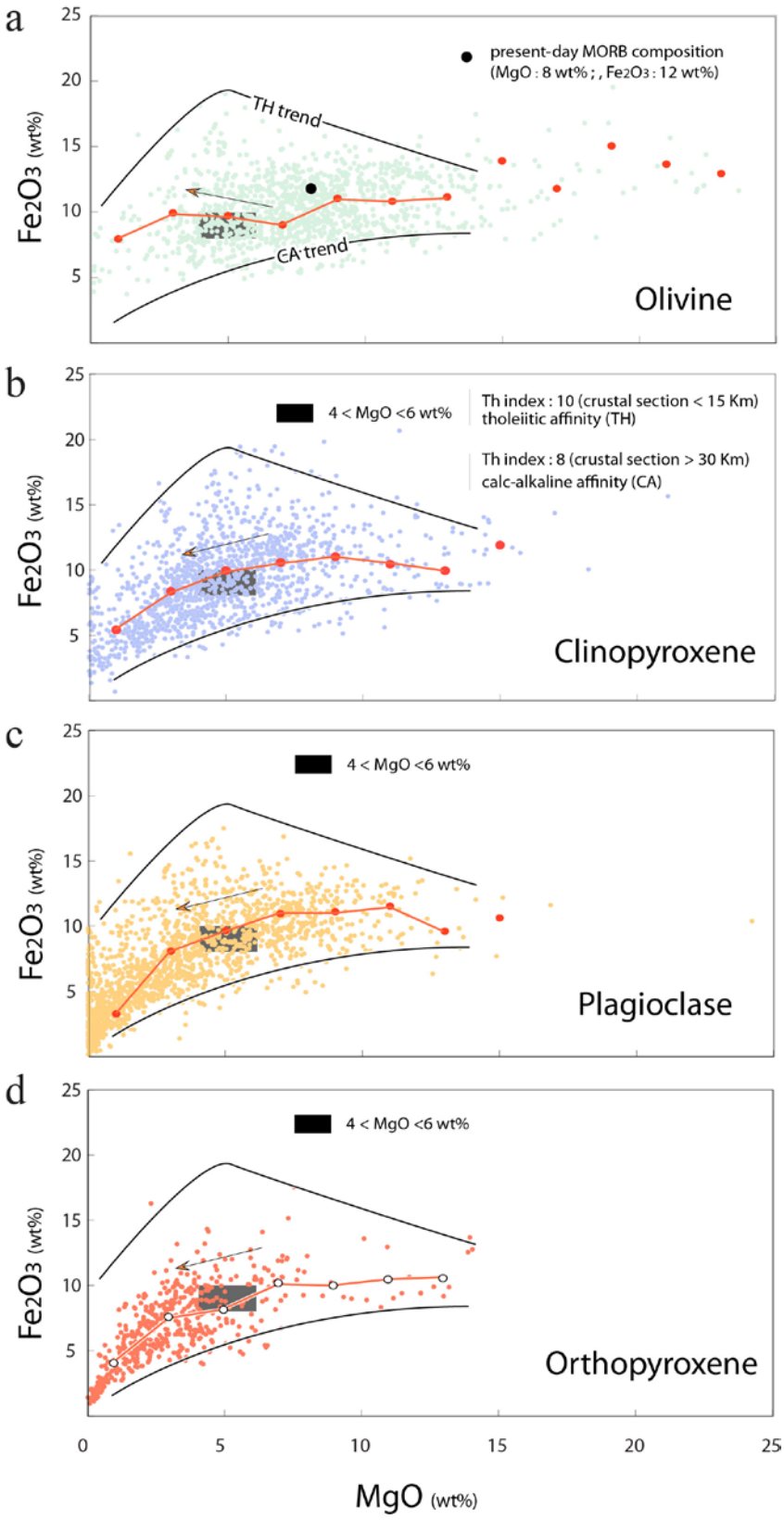

Figure 11 SI. Fe_2O_3 $_{total}$ – MgO (wt%) plot showing tholeiitic and calc-alkaline trend for magmatic rocks (continental setting) hosting olivine (a), clinopyroxene (b), plagioclase (c) and orthopyroxene. Condition of equilibrium between mineral and magma have been checked (c.f. Figure 2 SI). No test of equilibrium for biotite (e) and clinoamphibole (f). The Fe-Mg magmatic minerals form a discontinuous series with the olivine stabilized

early, followed by the growth of pyroxene then amphibole and biotite if water is available in the magma. Figure (a) shows that olivine-bearing magma dominantly evolves (red arrow) along a tholeiitic trend (red curves ; statistical assessment) within thin crust (< 15 Km, considering the elevated Th index; Chiaradia, 2014). In contrast, during slow ascent through a thick and/or cooler and/or hydrated continental lithosphere, sequential crystallization and separation of minerals cause the basaltic melt to evolve toward a progressively more calc-alkaline, Si-rich, composition. Clinopyroxene and plagioclase start to crystallize earlier and at higher-pressure than olivine and orthopyroxene. As MgO is incorporated into the clinopyroxene, the residual melt in calc-alkaline basalts tends to have a lower MgO content. In addition, as pressure promotes the incorporation of Ca in plagioclase the basaltic melt is depleted in Ca when it approaches the surface. Continued fractionation at lower pressure leads to crystallization of low-Ca orthopyroxene, low-Mg clinopyroxene, and low-Ca plagioclase resulting in magmatic rocks of dacitic and rhyolitic composition (c.f. Figure 10 SI). Though in calc-alkaline magma the memory of mantle temperature is largely lost, the compositional trends in pyroxene and feldspar can inform about the thermal state of the lithosphere. (e, f) Biotite and amphibole, forming in the uppermost levels of the lithosphere will dominantly evolve along calc-alkaline trends.

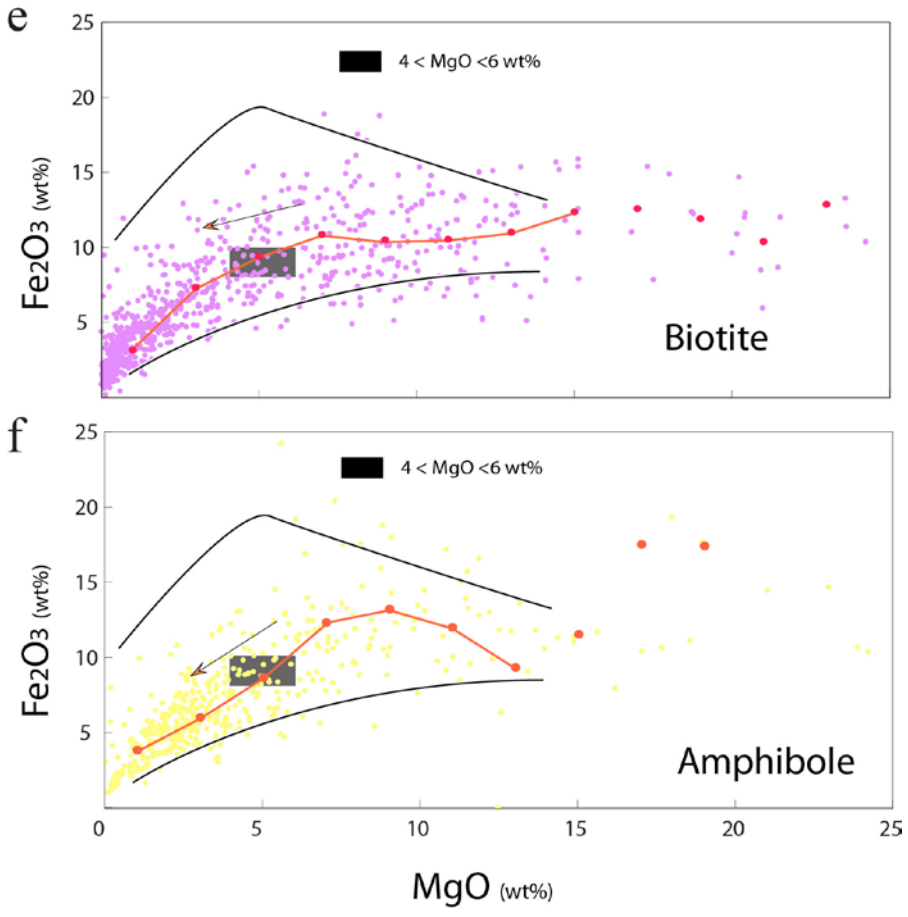

Figure 11 SI (to be continued)**.**

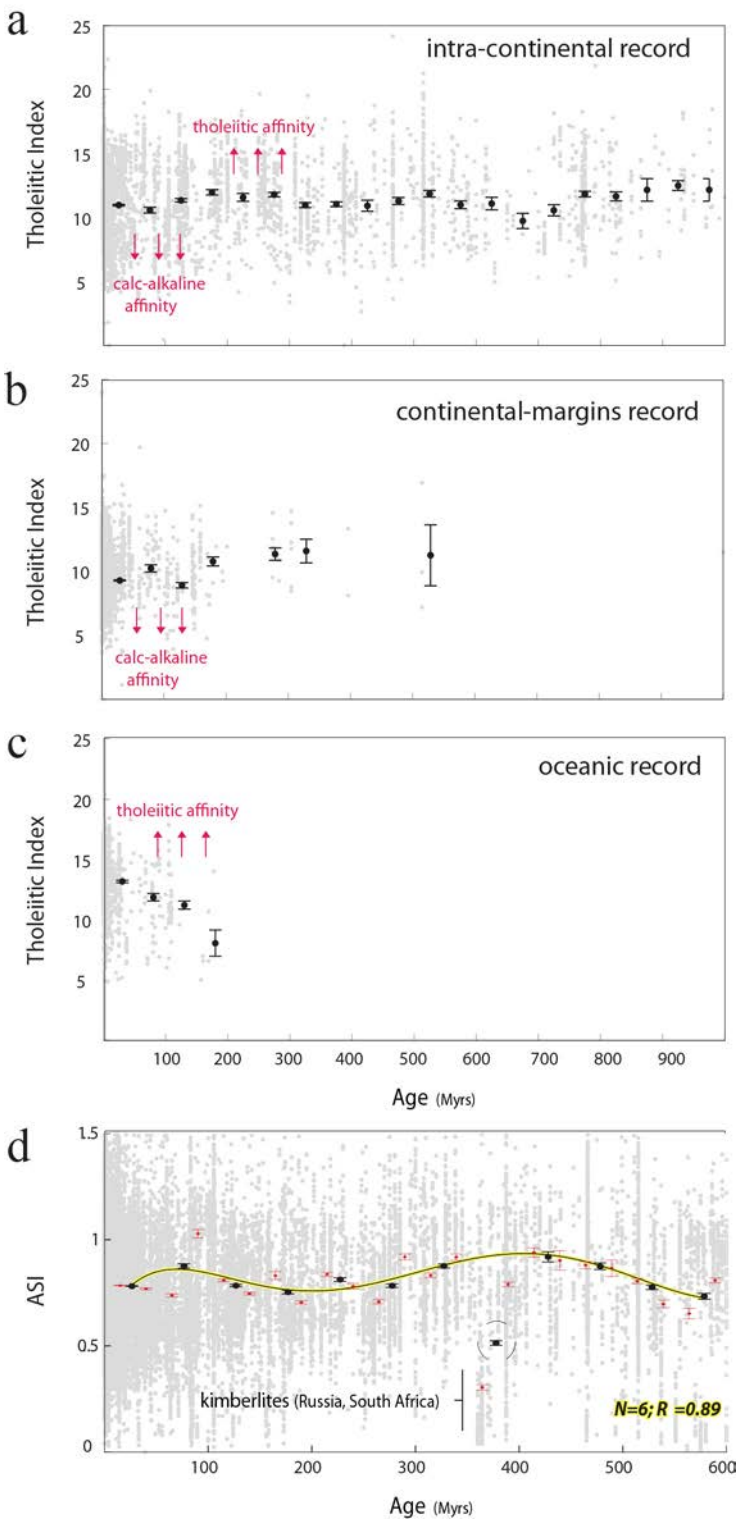

Figure 12 SI. (a,b,c) Time correlation between the gradual occurrence or decrease (statistical assessment) of tholeiitic magmas (Th Index : more Fe_2O_3 $_{total}$-enriched at MgO ~4-6 wt%, Miyashiro, 1974; Chiaradia, 2014) and the geological setting where magmas took place (> 8,500 data). (d) Aluminium Saturation Index (ASI ; mol. Al_2O_3 / [$CaO+Na_2O+K_2O$]) evolution of magmas (continental margins and intra-continental record) since 600 Myr (> 40,000 data). A polynomial curve (yellow) fitting the bootstrapped values (1000 draws, threshold value of 3, age step of 50 Myrs) was reported on the graph.

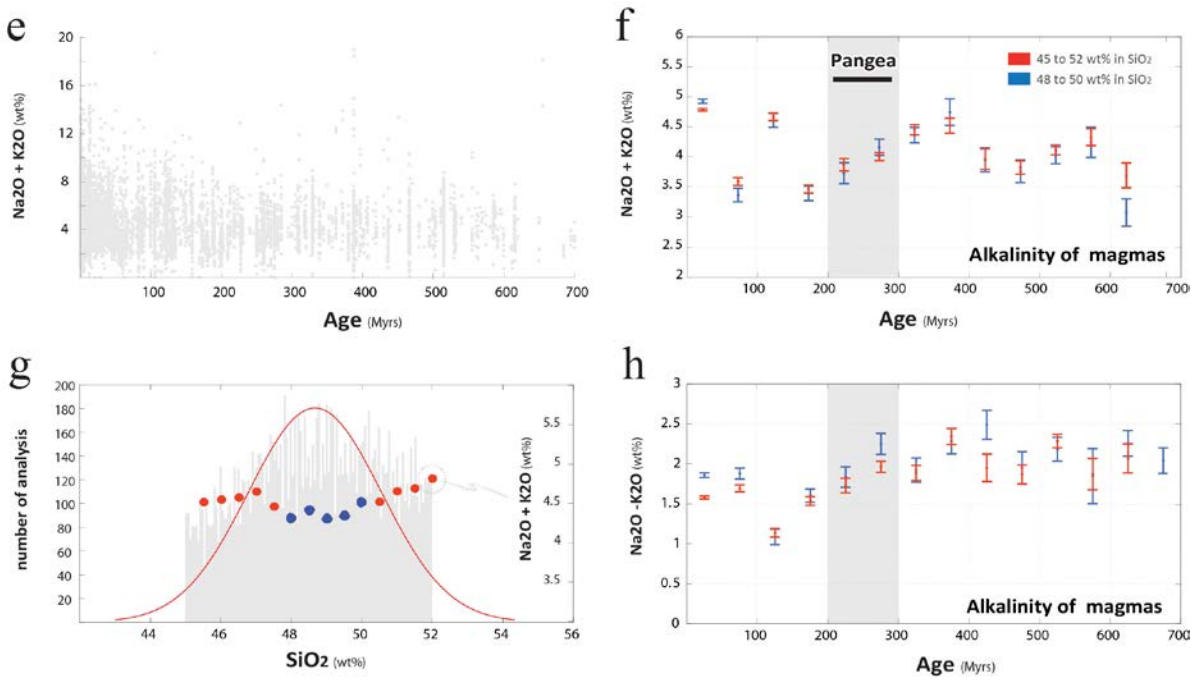

Figure 12 SI (to be continued). (e, f) Time correlation between the gradual occurrence or decrease (statistical assessment) of alkali magmas, with basaltic composition ($SiO_{2\ 45\text{-}52\ wt\%}$) in the continental record. The alkalinity of magma is given by the relative proportion of $Na_2O + K_2O$ mass percent (wt%) of rocks throughout their SiO_2 evolution (total-alkalis versus silica diagram : TSA). The red and blues points correspond to sub-alkali to alkali magmas with $SiO_{2\ 45\text{-}52\ wt\%}$ (> 15,000 data) and $SiO_{2\ 48\text{-}50\ wt\%}$ (> 3,600 data), respectively. (g) Bootstrapping of the total-alkalis content reveals a positive correlation between [$Na_2O + K_2O$] and SiO_2 in the more evolved composition of basaltic magmas ($SiO_{2\ >50\ wt\%}$). Basaltic magmas with evolved composition are not dominant in the database ; the distribution of SiO_2, given by the grey histograms in caption (h), shows a peak in composition occurring for $SiO_{2\ 48\text{-}50\ wt\%}$. A "bell" curve (red), fitting the Gaussian distribution, was reported on the graph. (h) Perspective view in the TSA diagram showing (statistical assessment) how sub-alkali to alkali basalts are divided into potassic trachybasalts and hawaiites, according to whether Na_2O-K_2O (wt%) is numerically less or greater than 2.0. The composition of basalts being described as "potassic" only when $K_2O > Na_2O$, i.e. Na_2O-$K_2O < 0$. Interestingly, the alkaline record is minimum at the time of Pangea supercontinent, suggesting that magma chambers stalled at shallow depth in the continental lithosphere (i.e. that is consistent with the tholeiitic signature of magma at that time). After ca. 200 Ma, the alkaline signature of basaltic magmas increases, suggesting a deepening of magmatic chambers in a thickening and cooling continental lithosphere (i.e. that is consistent with the calc-alkaline signature of magma at that time).

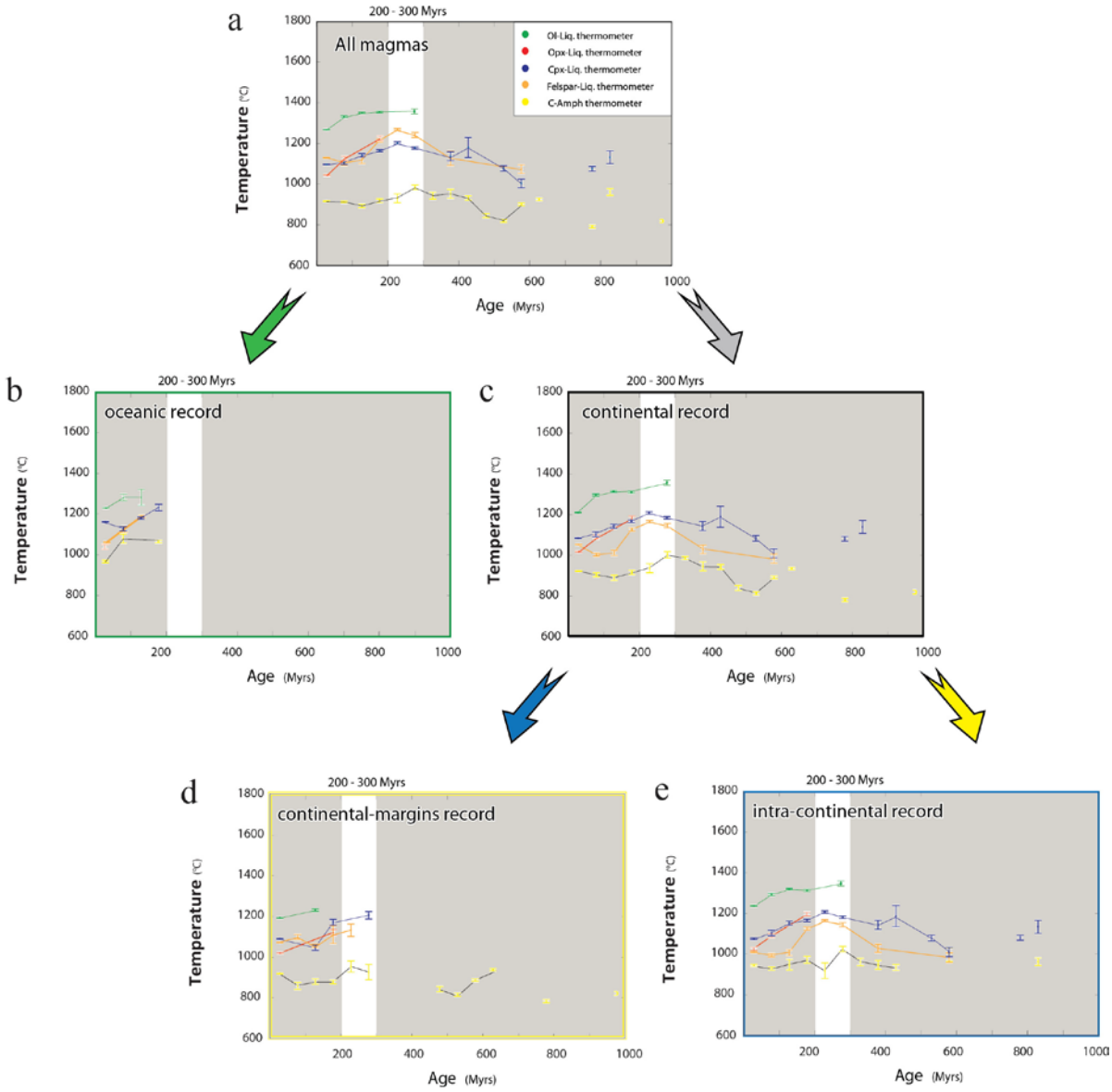

Figure 13 SI. (a) Range of T conditions of crystallization vs time for magmatic minerals sampled in (b) oceanic lithospheres and (c) continental lithospheres, including (d) continental-margins and (e) intra-continental settings, since 1 Gyrs.

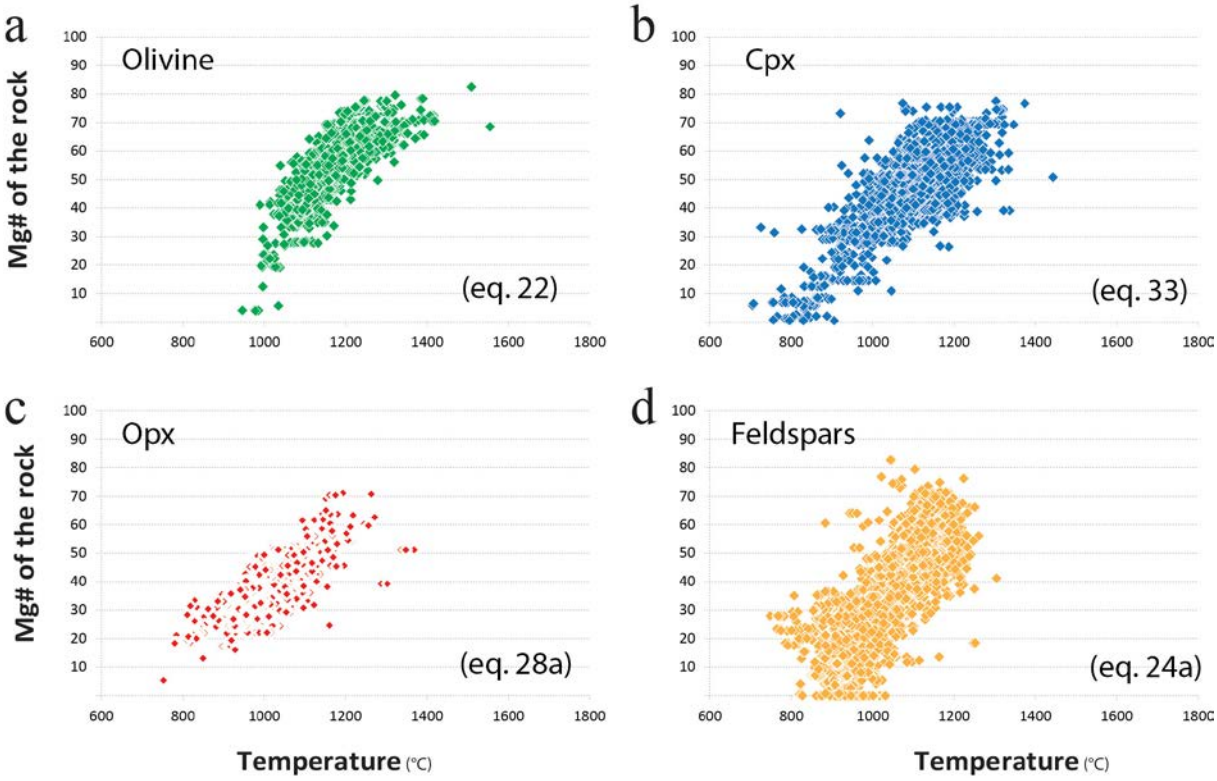

Figure 14 SI. T conditions of magmatic mineral crystallization obtained with different thermometers (Putirka, 2008) and plotted against the chemical composition of the hosting magma. Data suggest that high-Mg / high-T olivine (a) and pyroxenes (b, c) are stable in Mg-rich composition of melts. (d) High-Ca / high-T felspars are dominantly growing within Ca –Mg- rich magma.

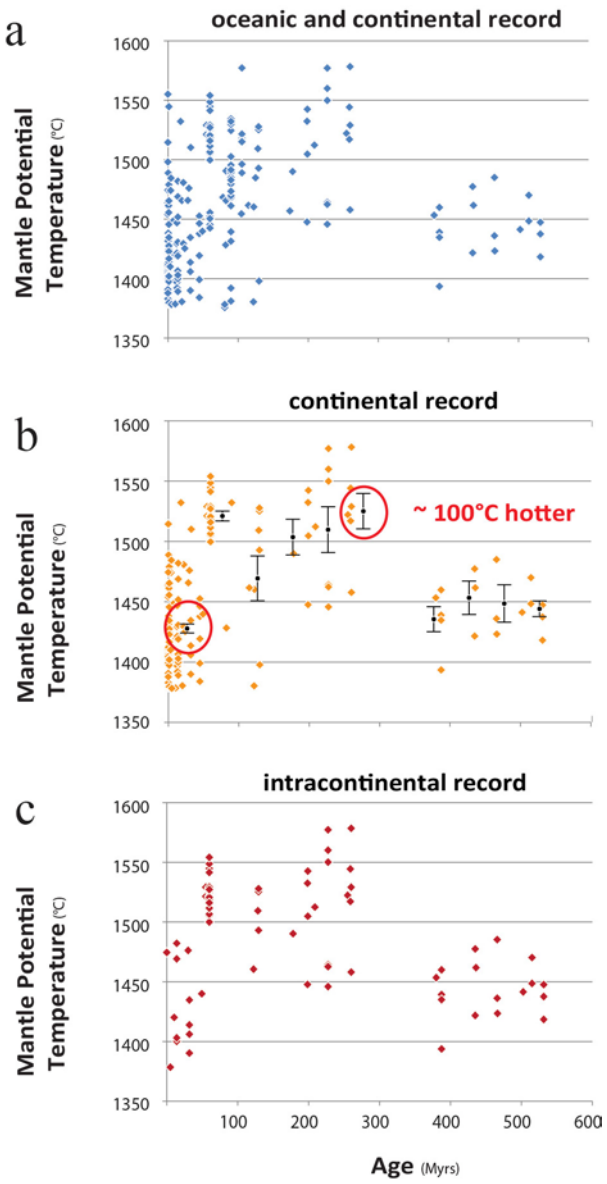

Figure 15 SI. Mantle potential temperature calculated with the PRIMELT3 MEGA software (Herzberg & Asimow, 2015). Data have been filtered according to their geodynamical setting.

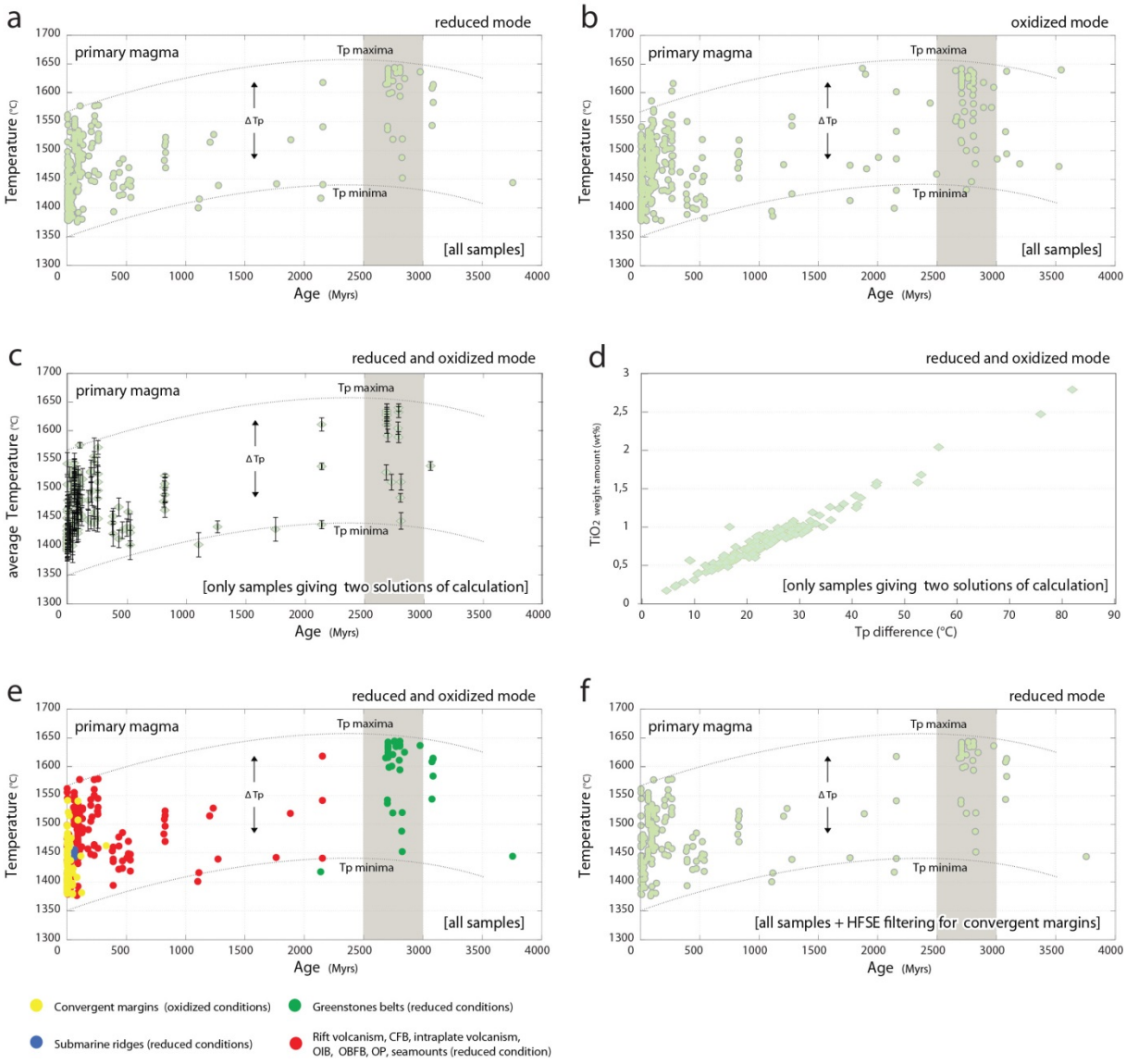

Figure 16 SI - Addressing redox conditions in the magmatic source. (a, b) Potential temperature (Tp) of mantle depicted from the composition of primary magmas (green points) using PRIMELT3 MEGA software (Herzberg & Asimow, 2015) and assuming reduced (Fe_2O_3/TiO_2=0.5 ; 271 data) and oxidized (Fe_2O_3/TiO_2=1 ;379 data) conditions in the source, respectively. 172 samples yielded solutions of calculation for both reduced and oxidized conditions (overlaps > 63%). (c,d) Uncertainties in Fe^{2+}/Fe_T propagate to uncertainties in mantle Tp lower than 30 °C for low-Ti type lavas (TiO_2<1 wt%) up to 80 °C for high-Ti types (TiO_2>2.5 wt%). In caption (e), Tps were broken in four groups corresponding to Arc-like (convergent margins), MORB-like (submarine ridges), Craton-like (greenstones belts) and Plume-like settings. This last group is likely to encompass: rift volcanism, continental flood basalts (CFB), intraplate volcanism, ocean-basin flood basalts (OBFB), ocean island basalts (OIB), oceanic plateaus (OP) and seamounts. Solutions of calculation have been obtained in reduced mode (Fe_2O_3/TiO_2=0.5), except for arc-related lavas (oxidized conditions). In (f), lavas formed in assumed arc-setting have been filtered on the basis of HFSE enrichments (Nb / Ta > 17, Stolz et al., 1996) and all solutions of calculation have been obtained in reduced mode.

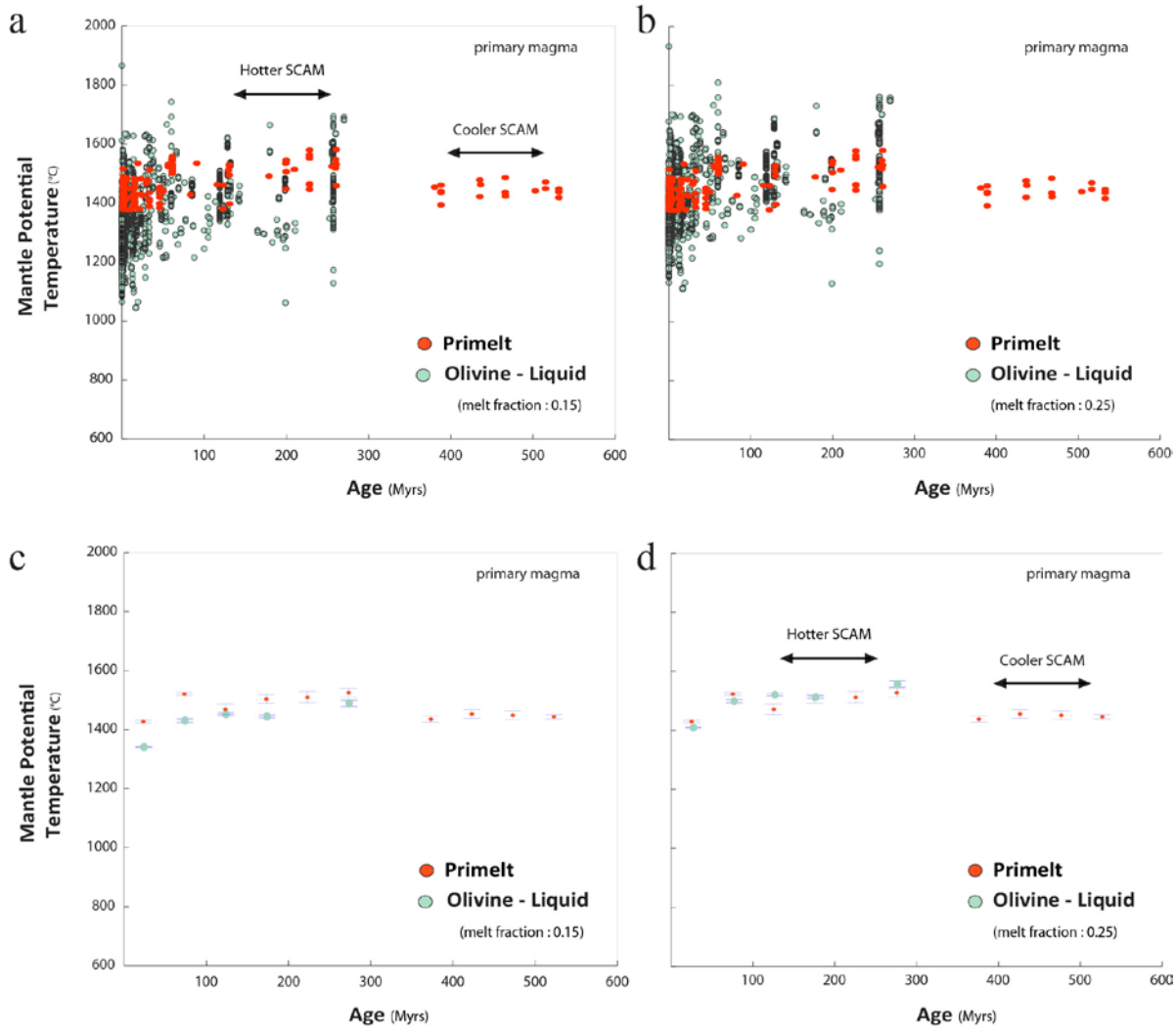

Figure 17 SI. Mantle potential temperature calculated with the Ol-Liq. method of Putirka (2008) using different values (0,25 and 0.15) of melt fraction (continental record). In red, mantle potential temperature calculated with the PRIMELT3 MEGA software (Herzberg & Asimow, 2015).Potential temperatures obtained with two independent methods, assuming melting by adiabatic decompression (PRIMELT) and/ or assisted by fluids in the mantle (Ol-Liq.), are thought to be representative of different thermal horizons in the upper mantle, ranging in depth from a shallow sublithospheric or subarc mantle, so-called ambient mantle (Tp minima) or SCAM, to a lower thermal boundary layer (Tp maxima) that, we infer, corresponds to the transition zone (410 - 660 Km). The difference of temperature between Tp maxima and minima (Δ Tp) calculated with PRIMELT (Figure 16 SI) is similar to the adiabatic temperature increase through the present-day upper mantle (~200°C) and, seemingly, has remained broadly constant since ~2.5 Gyrs. Accordingly, we suggest that the upper mantle differenced early as a single thermal and chemical layer, leading to the isolation and preservation of a geochemically primitive lower mantle. A progressive but limited decrease of ~100°C is proposed since ~2.5 Gyrs for this upper chemical reservoir. We infer that insulation of this reservoir beneath growing supercontinents leads to the generation of mantle plume-like clusters with elevated Tp values (e.g. the ca. 300 Myrs thermal event generated by Pangea), impacting the distribution of temperature gradients in the upper mantle without modifying the secular trend of cooling for Tp minima and maxima.

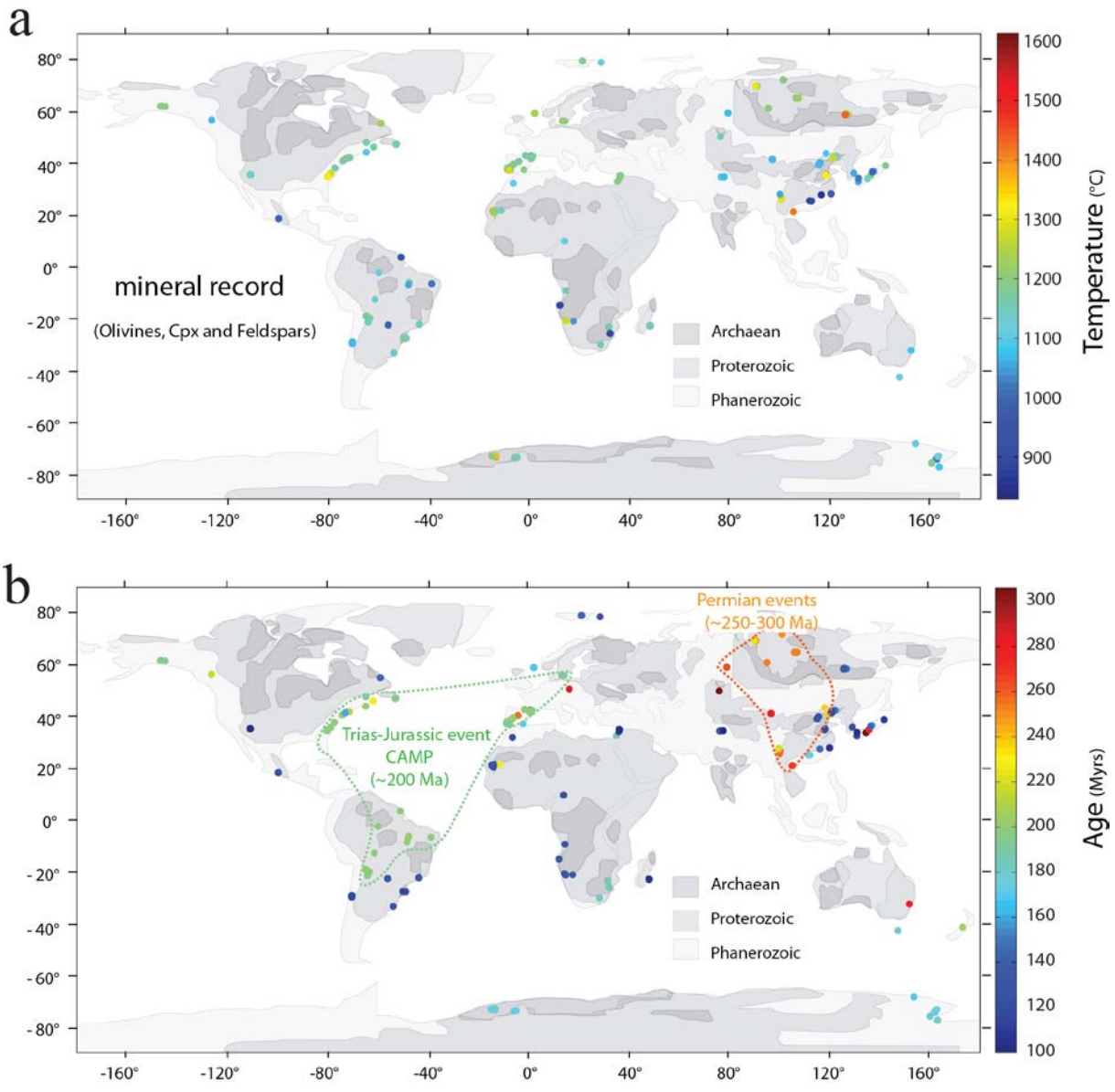

Figure 18 SI. (a) Distribution of magmatic rocks (continental setting) that yielded temperature estimates. T values were obtained with the Ol.-Liq., Cpx-Liq. and Feldspar-Liq. methods of Putirka (2008). (b) A few of the largest igneous provinces are broadly contoured (by the green and orange dashed lines) on this geological map, which depicts crustal geologic provinces as seen in seismic refraction and petrological data (Artemieva et al., 2006). No clear temporal or spatial zonation of temperature can be established within these domains.

References

Allen, J.C., and Boettcher, A.L. The stability of amphibole in andesite and basalt at high pressures. *Am. Mineral.* **68**, 307–314 (1983).

Anderson, D.L.,The thermal state of the upper mantle: no role for mantle plumes. *Geophysical Research Letters*, **27**, 3623-3626 (2000).

Anderson, J.L., Smith, D.R. The effects of temperature and fO2 on the Al-in-hornblende barometer. *Am. Mineral.* **80**, 549–559 (1995).

Anderson, J.L., Barth, A.P., Wooden, J.L., Mazdab, F. Thermometers and thermobarometers in granitic systems. *Rev. Mineral. Geochem.* **69**, 121–142 (2008).

Annen, C., Blundy, J., Sparks, R. The Genesis of Intermediate and Silicic Magmas in Deep Crustal Hot Zones.*J. of Petrology***47**, 505–539 (2006).

Artemieva I.M.Global 1°x1° thermal model TC1 for the continental lithosphere: implications for lithosphere secular evolution. Tectonophysics, **416**, 245-277 (2006).

Atherton, M., Petford, N. Generation of sodium rich magmas from newly underplated basaltic crust. *Nature***362**, 144–146 (1993).

Bachmann, O, Dungan, M.. Temperature-induced Al-zoning in hornblendes of the Fish Canyon magma, Colorado. *Am. Mineral.* **87**, 1062–1076 (2002).

Barclay, J., and Carmichael, I.S.E. A hornblende basalt from western Mexico: Water-saturated phase relations constrain a pressure-temperature window of eruptibility J. of Petrology **45**, 485-506 (2004).

Bédard, J., A catalytic delamination-driven model for coupled genesis of Archaean crust and sub-continental lithospheric mantle. *Geochimica et Cosmochimica Acta*, **70**, 1188-1214 (2006).

Blundy, J.D., Holland, T.J.B. Calcic amphibole equilibria and a new amphibole-plagioclase geothermometer. Contrib. Mineral. Petrol. 104, 208–224 (1990).

Buda, G., Koller, F., Kovacs, J., Ulrych, J. Compositional variation of biotite from Variscan Granitoids in Central Europe : A statistical evaluation. Acta Mineralogica-Petrographica, 45, 21-37 (2004).

Chung, S.L. & Jahn B.M.Plume–lithosphere interaction in generation of the Emeishan flood basalts at the Permian–Triassic boundary. Geology, 23, 889–892 (1995).

Chiaradia, M. Copper enrichment in arc magmas controlled by overriding plate thickness. *Nat. Geosci.* **7**, 43–46 (2014).

Clemens, J., Helps, P., Stevens, G. Chemical structure in granitic magmas - a signal from the source ?*Earth and Env.Sci. Trans. of the Royal Soc. of Edinburgh***100**, 159–172 (2010).

Coogan, L.A., Wilson, R.W., Gillis, K.M. & MacLeod, C.J. Near-solidus evolution of oceanic gabbro : Insight from amphibole geochemistry. *Geochim. Cosmochim. Acta* **65**, 4339-4357 (2001).

Courtillot, V., A. Davaille, J. Besse, and J. Stock. Three distinct types of hotspots in the Earth's mantle. *Earth and Planetary Science Letters*, **205**, 295–308 (2003).

Davidson, J. Turner, S, Handley, H., Macpherson, C and Dosseto, A. Amphibole "sponge" in arc crust? *Geology* **35**, 87-790 (2007).

Davidson, J., Turner, S., Plank, T. Dy/Dy*: Variations arising from mantle sources and petrogenetic processes. J. of Petrology **54**, 525-537 (2013).

Davies, G.F. Effect of plate bending on the Urey ratio and the thermal evolution of the mantle. *Earth and Planetary Science Letters*, **287**, 513–518 (2009).

Deer W. A., Howie R. A. & Zussman J. An Introduction to the Rock-Forming Minerals (2nd edition). Longman, Harlown(1992).

Dessimoz, M., Müntener, O., Ulmer, P. A case for hornblende dominated fractionation of arc magmas: the Chelan Complex (Washington Cascades). Contrib. Mineral. Petrol. 163, 567–589 (2012).

DePaolo, D. A Neodymium and Strontium isotopic study in the Mesozoic Calc-Alkaline Granitic Batholiths of the Sierra Nevada and Peninsular Ranges, California.*J.Geoph.Res.***86**, 10470–10488 (1981).

Dungan, M., Davidson, J. Partial assimilative recycling of the mafic plutonic roots of arc volcanoes : an example from the Chilean Andes. *Geology***32**, 773–776 (2004).

Erdmann, S., Martel, C., Pichavant, M., Kushnir, A. Amphibole as an archivist of magmatic crystallization conditions: problems, potential, and implications for inferring magma storage prior to the paroxysmal 2010 eruption of Mount Merapi, Indonesia. *Contrib. Mineral. Petrol.* **167**, 1-23 (2014).

Ernst, R.E. Large Igneous Provinces. Cambridge University Press, 653 p. (2014).

Ernst, W.G. Archean plate tectonics, rise of Proterozoic supercontinentality and onset of regional, episodic stagnant-lid behavior : Gondwana Research, **15**, 243-253 (2009).

Frost, D.J. & McCammon, C., 2008. The Redox State of Earth's Mantle. *Annu. Rev. Earth Planet. Sci.* **36**, 389-

Giesting, P.A., and Filiberto, J. Quantitative models linking igneous amphibole composition with magma Cl and OH content. Am. Mineral. **99**, 852-865 (2014).

Glazner, A. Thermal limitations on incorporation of wall rock into magma. *Geology***35**, 319-322 (2007).

Grigné, C., Labrosse, S., and Tackley, P.J., Convective heat transfer as a function of wavelength. Implications for the cooling of the Earth, *Journal of Geophysical Research* 110, B03409, 2005.

Grove, T.L. et al. Fractional crystallization and mantle-melting controls on calc-alkaline differentiation trends. *Contrib. Mineral. Petrol.* **145**, 515–533 (2003).

Harker, A. The Natural History of Igneous Rocks. London: Methuen (1909).

Hammarstrom, J.M., Zen, E.A.. Aluminium in hornblende: an empirical igneous geobarometer. *Am. Mineral*. **71**, 1297–1313 (1986).

Holland, T. J. B. and Blundy, J.D. Non-ideal interactions in calcic amphiboles and their bearing on amphibole-plagioclase thermometry. *Contrib. Mineral. Petrol*. **116**, 433–447 (1994).

He et al. Age and duration of the Emeishan flood volcanism, SW China: Geochemistry and SHRIMP zircon U–Pb dating of silicic ignimbrites, post-volcanic Xuanwei Formation and clay tuff at the Chaotian section. Earth Planet. Sci. Lett., 255, 306-323 (2007).

Herzberg, C., Asimow, P.D., 2008, Petrology of some oceanic island basalts: PRIMELT2. XLS software for primary magma calculation. Geochem. *Geochemistry Geophysics Geosystems*, v. 8, doi:10.1029/2008GC002057.

Herzberg, C., Asimow, P.D., 2015, PRIMELT3 MEGA.XLSM software for primary magma calculation: Peridotite primary magma MgO contents from the liquidus to the solidus. *Geochemistry Geophysics Geosystems*, v. 16, doi: 10.1002/2014GC005631.

Herzberg, C., Condie, K., and Korenaga, J. Thermal history of the Earth and its petrological expression. *Earth and Planetary Science Letters*, **292**, 79-88 (2010).

Herzberg, C., Gazel, E. Petrological evidence for secular cooling in mantle plumes. Nature, **458**, 619-622 (2009).

Hildreth, W., Moorbath, S. Crustal contributions to arc magmatism in the Andes of Central Chile. *Contrib. Mineral.Petrol.***98**, 455–489 (1988).

Holland, T. J. B. and Blundy, J.D. Non-ideal interactions in calcic amphiboles and their bearing on amphibole-plagioclase thermometry. Contrib. Mineral. Petrol. 116, 433–447 (1994).

Hollister, L.S., Grissom, G.C., Peters, E.K-, Stowell, H.H., and Sisson. Confirmation of the empirical correlation of Al in hornblende with pressure of solidification of calc-alkaline plutons. *Am. Mineral*.**72**, 231-239 (1987).

Humphreys, M., Christopher, T., Hards, V. Microlite transfer by disaggregation of mafic inclusions following magma mixing at Soufriere Hills volcano, Montserrat. *Contrib. Mineral. Petrol.* **157**, 609–624 (2009).

Husson, L. & Conrad, C.P. (2012) On the location of hotspots in the framework of mantle convection : Geophysical Research Letters,v. 39, L17304, doi:10.1029/2012GL052866.

John, T., Klemd, R., Klemme, S., Pfänder, J.A., Hoffmann, J.E. Gao, J. Nb–Ta fractionation by partial melting at the titanite–rutile transition. *Contrib. Mineral. Petrol.* **161**, 35–45 (2011).

Johnson, M. C., and Rutherford, M. J. Experimental calibration of the aluminum-in-hornblende geobarometer with application to Long Valley Caldera (California) volcanic rocks. *Geology* **17**, 837–841 (1989).

Katsura, T., Yoneda, A., Yamazaki, D., Yoshino, T., Ito, E. Adiabatic temperature profile in the mantle. Physics of the Earth and Planetary Interiors, 183, p. 212–218 (2010).

Keller, C.B. & Schoene, B. Statistical geochemistry reveals disruption in secular lithospheric evolution about 2.5 Gyr ago. *Nature* **485**, 490–493 (2012).

Kent, A. J. R. Preferential eruption of andesitic magmas: Implications for volcanic magma fluxes at convergent margins. *Geol. Soc. London* **385**, 257-280 (2014).

Kiss, B., Harangi, S., Ntaflos, T., Mason, P.D., Pal-Molnar, E. Amphibole perspective to unravel pre-eruptive processes and conditions in volcanic plumbing systems beneath intermediate arc volcanoes: a case study from Ciomadul volcano (SE Carpathians). *Contrib. Mineral. Petrol*. **167**,1-27 (2014).

Klemme, S, Blundy, J.D., Wood, B.J. Experimental constraints on major and trace element partitioning during partial melting of eclogite. *Geochim Cosmochim Acta* **66,** 3109–3312 (2002).

Korenaga, J., Archean geodynamics and the thermal evolution of Earth. In: Benn, K., Mareschal, J.-C., Condie, K. (Eds.), Archean Geodynamics and Environments. American Geophysical Union, **164**. 7–32 (2006).

Kratzmann, D.J., Carey, S., Scasso, R.A., and Naranjo, J.-A. Role of cryptic amphibole crystallization in magma differentiation at Hudson volcano, Southern Volcanic Zone, Chile. Contrib. Mineral. Petrol. **159**, 237-264 (2010).

Labrosse, S., Jaupart, C. Thermal evolution of the Earth: secular changes and fluctuations of plate characteristics. *Earth Planet. Sci. Lett*. 260, 465–481 (2007).

Lange, R.A., Carmichael I.S.E. Densities of Na_2O-K_2O-MgO-MgO-FeO-Fe_2O_3-Al_2O_3-TiO_2-SiO_2 liquids: New measurements and derived partial molar properties. *Geochim. Cosmochim. Acta*, **51**, 2931-2946 (1987).

Lee, C-T. A., Lee, T. C. & Wu, C-T.Modeling the compositional evolution of recharging, evacuating, and fractionating (REFC) magma chambers: Implications for differentiation of arc magmas.*Geochim.Cosmochim.Acta*; DOI: 10.1016/j.gca.2013.08.009 (2013).

Li, Z.-X.A, Lee, C-T.A. The constancy of upper mantle fO2 through time inferred from V/Sc ratios in basalts. *Earth Planet. Sci. Lett.* **228**, .483–93 (2004).

Mamani, M., Wörner, G., and Sempere, T. Geochemical variations in igneous rocks of the Central Andean orocline (13°S to 18°S): Tracing crustal thickening and magma generation through time and space. *Bull. Geol. Soc. Am*. **122**, 162 – 182 (2010).

Miyashiro, A. Volcanic rock series in island arcs and active continental margins.Am. *J. Sci.***274**, 321-355 (1974).

Moulas, E., Burg, J.-P ., Podladchikov, Y. Stress field associated with elliptical inclusions in a deforming matrix: Mathematical model and implications for tectonic overpressure in the lithosphere. *Tectonophysics*; DOI: 10.1016/j.tecto.2014.05.004 (2014).

O'Neil J., Francis D., Carlson R.W. Implications of the Nuvvuagittuq greenstone belt for the formation of Earth's early crust. *J. Petr*. **52**, 985–1009 (2011).

Pearce J.A., Peate D.W. Tectonic implications of the composition of volcanic arc magmas. *Annu. Rev. Earth Planet. Sci.* **23**, 251–285 (1995).

Pichavant, M, Martel, C, Bourdier, J-L, Scaillet, B. Physical conditions, structure, and dynamics of a zoned magma chamber: mount Pelée (Martinique, Lesser Antilles Arc). *J. Geophys. Res*. **107**, 1–28 (2002).

Putirka, K.D. Thermometers and barometers for volcanic systems, in Putirka, K.D., and Tepley, F., eds. Minerals, inclusions and volcanic processes. *Mineralogical Society of America Reviews in Mineralogy and Geochemistry* **69**, 61–120 (2008).

Putirka, K. Amphibole thermometers and barometers for igneous systems, and some implications for eruption mechanisms of felsic magmas at arc volcanoes. Am. Mineral. 10.2138/am-2016-5506 (2016).

Rey, P. From lithospheric thickening and divergent collapse to active continental rifting. Journal of the Geological Society, Special Publication 184, 77-88 (2001).

Ridolfi, F. & Renzulli, A. Calcic amphiboles in calc-alkaline and alkaline magmas: thermobarometric and chemometric empirical equations valid up to 1,130°C and 2.2 GPa. *Contrib. Mineral. Petrol*. **163**, 877–895 (2012).

Righter, K.; Carmichael, I. S. E.Phase equilibria of phlogopite lamprophyres from western Mexico: biotite-liquid equilibria and P- T estimates for biotite-bearing igneous rocks. Contributions to Mineralogy and Petrology **123**, 1-21 (1996).

Rutherford, M.J., and Devine, J.D. Magmatic conditions and magma ascent as indicated by hornblende phase equilibria and reactions in the 1995--2002 Soufrière Hills magma. J. of Petrology **44**, 1433-1454 (2003).

Schmidt, M. W. Amphibole composition in tonalite as a function of pressure: An experimental calibration of the Al-in-hornblende barometer. *Contrib. Mineral. Petrol*. **110**, 304–310 (1992).

Smith, D.J. Clinopyroxene precursors to amphibole sponge in arc crust. Nat. Commun. 5, 4329; DOI:1038/ncomms5329 (2014).

Shane, P, Smith, V.C. Using amphibole crystals to reconstruct magma storage temperatures and pressures for the post-caldera collapse volcanism at Okataina volcano. *Lithos* **156–159**, 159–170 (2013).

Sisson, T. W. & Bacon, C. R. Gas-driven filter pressing in magmas. *Geology***27**, 613–616 (1999).

Sisson, T.W., Grove, T.L. Experimental investigations of the role of H2O in calc-alkaline differentiation and subduction zone magmatism. *Contrib. Mineral. Petrol.* **113**, 143–166 (1993).

Spera, F., Bohrson, W.. Energy constrained open system magmatic processes I : general model and energy-constrained assimilation and fractional crystallisation (EC-AFC) formulation. *J. of Petrology***42**, 999–1018 (2001).

Stolz, A.J., Jochum, K.P., Spettel, B., Hofmann, A.W. Fluid- and melt-related enrichment in the subarc mantle: Evidence from Nb/Ta variations in island-arc basalts. *Geology* **24**, 587-590 (1996).

Tang, M., Chen, K., Rudnick, R.L. Archean upper crust transition from mafic to felsic marks the onset of plate tectonics. Science, 351, 372-375 (2016).

Tajčmanová, L et al. Grain-scale pressure variations and chemical equilibriumin high-grade metamorphic rocks. *J. Metamorphic Geology* **32**, 195–207 (2014).

Tepper, J.H., Nelson, B., Bergantz, G., Irving, A. Petrology of the Chiilwack batholith, North Cascades, Washington. Generation of calc-alkaline granitoids by melting of mafic lower crust with variable water fugacity.*Contrib. Mineral.Petrol.***113**, 333–351 (1993).

Tindle, A.G. & Webb, P.C. Probe-AMPH—A spreadsheet program to classify microprobe-derived amphibole analyses. *Computers & Geosciences* **20**, 1201–1228 (1994).

Tribuzio, R., Renna, M.R., Dallai, L., Zanetti, A. The magmatic–hydrothermal transition in the lower oceanic crust: Clues from the Ligurian ophiolites, Italy. Geochim. Cosmochim. Acta 1**30**, 188-211 (2014).

Turner, S., Caulfield, J.T., Rushmer, T., Turner, M.B., Cronin, S.J., Smith, I., and Handley, H.K. Magma evolution in the primitive, intra-oceanic Tonga arc: Rapid pretrogenesis of dacites at Fonualei Volcano. J. of Petrology **53,** 1231-1253 (2012).

Xu et al. Zircon U–Pb and Hf isotope constraints on crustal melting associated with the Emeishan mantle plume. Geochimica et Cosmochimica Acta, 72, 3084-310 (2008)

Yücel, C., Arslan, M., Temizel, I.,Abdioğlu, E. Volcanic facies and mineral chemistry of Tertiary volcanics in the northern part of the Eastern Pontides, northeast Turkey: implications for pre-eruptive crystallization conditions and magma chamber processes. *Miner. Petrol.* **108**, 439-467 (2013).